

University of Mississippi

eGrove

---

Electronic Theses and Dissertations

Graduate School

---

8-1-2022

## Low-Velocity Impact, Vibration and Shock Response of Unstitched/Stitched E- And S- Glass/Vinyl Ester Composites

Shahriar Chowdhury

Follow this and additional works at: <https://egrove.olemiss.edu/etd>

---

### Recommended Citation

Chowdhury, Shahriar, "Low-Velocity Impact, Vibration and Shock Response of Unstitched/Stitched E- And S- Glass/Vinyl Ester Composites" (2022). *Electronic Theses and Dissertations*. 2361.  
<https://egrove.olemiss.edu/etd/2361>

This Thesis is brought to you for free and open access by the Graduate School at eGrove. It has been accepted for inclusion in Electronic Theses and Dissertations by an authorized administrator of eGrove. For more information, please contact [egrove@olemiss.edu](mailto:egrove@olemiss.edu).

LOW-VELOCITY IMPACT, VIBRATION AND SHOCK RESPONSE OF UNSTITCHED/  
STITCHED E- AND S- GLASS/VINYL ESTER COMPOSITES

A Thesis

Presented for the

Master of Science

Degree

The University of Mississippi

Shahriar Chowdhury

August 2022

Copyright © 2022 by Shahriar Chowdhury  
All rights reserved

## ABSTRACT

In this study, the effects of through-thickness stitching on the dynamic properties, low-velocity impact and shock responses of stitched and unstitched E- and S- Glass/Vinyl Ester composites have been investigated. The stiffness and loss factor (inherent damping) properties are obtained from impulse-frequency response experiments using the hammer excitation method. Drop weight impact testing machine was used to carry out low-velocity punch shear tests on the composite specimens following ASTM D3763 Standard, and shock tube apparatus was used to determine center point deflection under blast loading. The stitching increased the dynamic flexural modulus by 13% for E- and 8% for S- Glass/Vinyl Ester composites but had minimal change in the case of loss factor. The stitching also demonstrated approximately 20% increase in total energy absorption and approximately 40% increase in fracture energy for E- Glass/Vinyl Ester while showing approximately 12% increase in total energy absorption and approximately 30% increase in fracture energy for S- Glass/Vinyl Ester. Under shock loading, the stitched E-Glass/Vinyl Ester specimens exhibited lowest center point deflection of 3.7 mm center point displacement, indicating greater resistance while the rest had values within the range of 4 mm to 4.5 mm. The average energy absorption up to the point of maximum deflection was higher for the unstitched specimens compared to their stitched counterparts.

## DEDICATION

This work is a culmination of efforts coupled with invaluable support from some invaluable individuals. Thus, I want to dedicate this thesis to those people who provided me the stepping stones towards achieving it successfully. This starts with my parents who I am forever indebted to and then my supervisor Dr. Prabhakar Raju Mantena whose guidance helped me every step of the way in finding my ground to conduct research in a foreign land. I am extremely grateful to my friends and mentors Suman Babu Ukyam and Dr. Damian Lee Stoddard as well as Mr. Paul

Matthew Lowe and would like to dedicate this to them as well.

## ACKNOWLEDGMENTS

This thesis would not have been possible without the continuous support and advice of Dr. Prabhakar Raju Mantena, Professor of Mechanical Engineering. I would also like to thank and acknowledge Dr. Suman Babu Ukyam and Dr. Damian Lee Stoddard for the amount of effort and time they have given every step of the way in helping me to achieve this. I would also like to acknowledge Mr. Paul Matthew Lowe, Supervisor of Machine shop, School of Engineering for his continuous help ranging from preparing samples to setting up and troubleshooting testing equipment.

I extend my acknowledgment and appreciation to my thesis committee members Dr. Yiwei Han, Professor of Mechanical Engineering and Dr. A. M. Rajendran, Chair and Professor of Mechanical Engineering for serving on the thesis committee as well as support throughout my Masters.

I would also like to thank and acknowledge the contribution made by ‘Srushti Engineering Innovations PVT. Ltd.’ (Bengaluru, India) towards the completion of this thesis. The shock tube apparatus supplied by them has proven to be a valuable asset in conducting shock loading experiments.

## TABLE OF CONTENTS

ABSTRACT.....	II
DEDICATION.....	III
ACKNOWLEDGEMENT.....	IV
TABLE OF CONTENTS.....	V
LIST OF FIGURES.....	VII
CHAPTER 1: INTRODUCTION.....	1
1.1 BACKGROUND AND MOTIVATION.....	1
1.2 RELEVANT LITERATURE REVIEW.....	4
1.3 OBJECTIVE AND SCOPE OF STUDY.....	10
1.3.1 SPECTRUM ANALYZER.....	11
1.3.2 LOW-VELOCITY IMPACT.....	11
1.3.3 SHOCK TUBE.....	11
CHAPTER 2: MATERIALS.....	12
2.1 MATERIAL USED.....	12
2.2 SPECIMEN PREPARATION.....	17
CHAPTER 3: EXPERIMENTAL PROCEDURE.....	18

3.1 VIBRATION EXPERIMENTAL PROCEDURE .....	18
3.2 LOW-VELOCITY EXPERIMENTAL PROCEDURE.....	25
3.3 SHOCK TUBE EXPERIMENTAL PROCEDURE.....	27
CHAPTER IV: RESULTS AND DISCUSSION .....	31
4.1 VIBRATION ANALYSIS.....	31
4.2 LOW-VELOCITY IMPACT ANALYSIS .....	36
4.3 SHOCK TUBE RESULT ANALYSIS.....	51
CHAPTER V: CONCLUSION.....	64
5.1 VIBRATION ANALYSIS.....	64
5.2 LOW-VELOCITY IMPACT .....	64
5.3 SHOCK ANALYSIS .....	65
5.4 RECOMMENDATION FOR FUTURE RESEARCH.....	66
REFERENCES .....	45
VITA.....	47

## LIST OF FIGURES

<b>Figure 1.</b> Bridge GFRP decks with steel girders hoisted for bridge construction (Friedberg bridge in Germany).....	2
<b>Figure 2.</b> FRP used in military vehicles (Sources: U.S. Air Force MSgt Donald R. Allen and General Dynamics Bath Iron Works).....	3
<b>Figure 3.</b> 3 stitched and 3 unstitched S-glass/vinyl ester woven composite panels (Courtesy: ERDC, Vicksburg) ...	13
<b>Figure 4.</b> 3 stitched and 3 unstitched E-glass/vinyl ester woven composite panels (Courtesy: ERDC, Vicksburg)...	14
<b>Figure 5.</b> Loop stitch (0.5inch width) with a gap of 2 inch in-plane directions.....	15
<b>Figure 6.</b> Specimens for vibration analysis cut from (a) Stitched, and (b) Unstitched E-Glass/Vinyl Ester composite panels.....	21
<b>Figure 7:</b> (a) Spectrum Analyzer (b) Signal Amplifier.....	22
<b>Figure 8.</b> Mounting the sample and attaching the accelerometer on the specimen.....	23
<b>Figure 9.</b> Tapping the specimen at the proper location in accordance with the desired FRF matrix element.....	24
<b>Figure 10.</b> CEAST 9450 drop weight impact system with pneumatic assist and data acquisition system dashboard matrix.....	26
<b>Figure 11.</b> Schematic of the incident and reflected wavefront travelling through the shock tube.....	28
<b>Figure 12.</b> Schematic of specimen mounting using flanges and camera location.....	30
<b>Figure 13.</b> Dynamic Flexural Modulus ( $E'$ ) and Loss Factor ( $\eta$ ) for each unstitched and stitched E- and S-Glass/Vinyl Ester specimens from vibration experiments.....	33
<b>Figure 14.</b> Dynamic Flexural Modulus ( $E'$ ) and Loss Factor ( $\eta$ ) for all types of specimens.....	34
<b>Figure 15.</b> Comparison of Force vs Time plots for (a) E- Glass/Vinyl Ester (b) S- Glass/Vinyl Ester and (c) between representative specimens of E- and S- Glass/Vinyl Ester samples from low velocity punch-shear tests.....	38
<b>Figure 16.</b> Comparison of Force vs Deflection plots for (a) E- Glass/Vinyl Ester (b) S- Glass/Vinyl Ester and (c) between representative specimens of E- and S- Glass/Vinyl Ester samples from low velocity punch- shear tests.....	40
<b>Figure 17.</b> Comparison of Energy vs Deflection plots for (a) E- Glass/Vinyl Ester (b) S- Glass/Vinyl Ester and (c) between representative specimens of E- and S- Glass/Vinyl Ester samples from low velocity punch- shear tests.....	42
<b>Figure 18.</b> Comparison of Force, Energy and Deflection plots among representative specimens of E- and S-Glass/Vinyl Ester samples from low velocity punch- shear tests.....	43
<b>Figure 19.</b> Comparison of (a) Peak load and (b) Deflection at peak load of the glass fiber reinforced specimens from low velocity punch-shear tests.....	45
<b>Figure 20.</b> Comparison of (a) Specific energy at damage initiation, (b) Specific energy at puncture propagation, and (c) Total specific energy absorption of E- and S-Glass/Vinyl Ester specimens from low velocity punch-shear tests.....	47
<b>Figure 21.</b> Comparison of Calculated Computed Fracture Energy of E- and S-Glass Vinyl Ester Specimens from low velocity punch-shear tests.....	48

<b>Figure 22.</b> Low-velocity punch-shear test specimens before and after impact: (a) Stitched S-Glass/Vinyl Ester, (b) Unstitched S-Glass/Vinyl Ester, (c) Stitched E-Glass/Vinyl Ester, and (d) Un-stitched E-Glass/Vinyl Ester. ....	50
<b>Figure 23.</b> Load-Time response of (a) Stitched E-Glass/Vinyl Ester, (b) Unstitched E-Glass/Vinyl Ester, (c) Stitched S-Glass/Vinyl Ester and (d) Unstitched S-Glass/Vinyl Ester (e) All specimens averaged under shock loading.....	53
<b>Figure 24.</b> Displacement-Time response of (a) Stitched E-Glass/Vinyl Ester, (b) Unstitched E-Glass/Vinyl Ester, (c) Stitched S-Glass/Vinyl Ester and (d) Unstitched S-Glass/Vinyl Ester (e) All specimens averaged under shock loading. ....	57
<b>Figure 25.</b> Load-Deflection response of (a) Unstitched S-Glass/Vinyl Ester, (b) Stitched S-Glass/Vinyl Ester, (c) Unstitched E-Glass/Vinyl Ester and (d) Stitched E-Glass/Vinyl Ester, and (e) All specimens averaged under shock loading. ....	60
<b>Figure 26.</b> Average center point acceleration of the composite specimens under shock loading. ....	62
<b>Figure 27.</b> Average center point acceleration of the composite specimens under shock loading. ....	63

# CHAPTER I

## INTRODUCTION

### **1.1 Background and Motivation**

With increased composite usage in industrial, aviation and aerospace sectors came the need for optimizing their strength and stiffness in order to facilitate a wide variety of applications. Composite materials are highly desired in structural applications due to their high specific strength and stiffness properties in contrast with their metallic counterparts. Even for concrete, where corrosion is of major concern, glass fiber reinforced polymer (GFRP) composites have proven to exhibit substantial benefits [1] as opposed to steel rebars due to their high-stiffness weight ratio, high strength-weight ratio, availability and resistance to environmental abrasion. In some cases, such as for marine applications, the GFRP have proven to be more durable than steel reinforcements but a key aspect of it are the damping properties. Where good damping and stiffness properties are required, GFRPs can provide exceptional support alongside other conveniences e.g., bridges. Figure 1 portrays the outcome of the above-mentioned positive aspects of GFRP compared to steel as a complete deck of a bridge in Germany is made out of E-Glass/Isophthalic polyester.

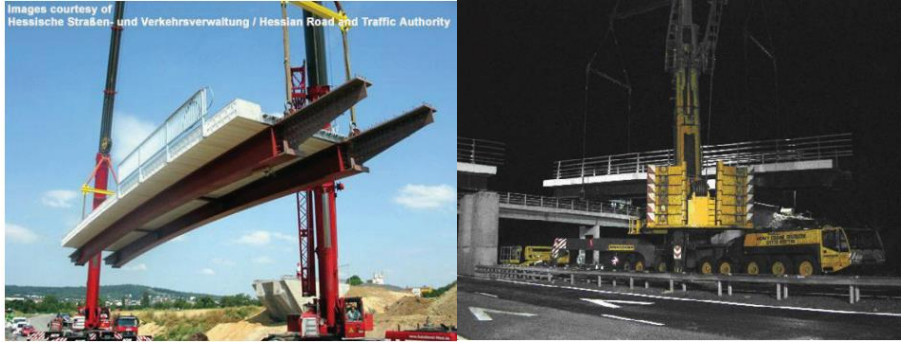


**Figure 1.** Bridge GFRP decks with steel girders hoisted for bridge construction  
(Friedberg bridge in Germany) [2]

One of the most notable applications of reinforced polymer matrix composites is in the aerospace and aeronautical industry. This stemmed from the need for high lift to weight ratio and better stiffness properties at high velocities while also providing greater durability and cutting down costs from metallic counterparts. The high maintenance and repair costs, coupled with susceptibility to chemical degradation also propelled the use of composites as fundamental building blocks for such advanced applications. The biggest advantage is the ability to resist impact at different energy absorption levels, particularly compressive loads; at a much lower percentage weight of the original metallic alloy constituent. FRPs have found significant applications in the military examples of which include fighter aircrafts [3] notable of which are: U.S. AV-8B, YF23, F-Series, B-2 Bomber etc.; European Harrier GR7, Mirage 2000, Rafael, Eurofighter etc.; Russian MIG 29, Su Series etc. and transport aircrafts such as KC135, C17, Boeing 777, Airbus A320, A380 etc. A couple of examples of military applications are shown in **Figure 2.**



**Figure 2.** FRP used in military vehicles (Sources: [Left] U.S. Air Force MSgt Donald R. Allen and [Right] General Dynamics Bath Iron Works)

Another noteworthy application of the fiber reinforced polymer composites would be the CPU motherboards and panels on-board military vehicles. This encompasses the need for all the types of experimentation described throughout this study i.e., vibration and load bearing capacity. This particular field of study had gained its significance during the past world wars where an otherwise unharmed vehicle would be rendered useless merely because of its control panel sustaining damage from enemy fire. The use of FRPs in such cases allowed the panels to maintain their integrity during operation despite coming under different types of loads while also providing excellent base for the circuitry involved. Aside from these major aspects, there are tons of other uses for the FRPs in significant commercial, military and aerospace application.

## 1.2 Relevant Literature Review

Various failure modes may occur in composite materials and cause damage, a brief overview of which has been given by Ghobadi [4]. But in some applications, they are susceptible to failure that may not be apparent upon superficial inspection and yet can catastrophically undermine the structural integrity of a system. This is of great concern particularly in the aerospace systems where losses incurred are greater in terms of cost and investments.

To account for this, different kinds of reinforcements have been realized. The most common type for improving in-plane properties is the inclusion of fiber reinforcement in the third direction (e.g., knitting, weaving, stitching) which modifies not only physical properties such as modulus, strength, viscoelasticity but also flammability and corrosion. [5]. The primary focus of these types of reinforcement is to increase failure prevention in the through thickness direction as it is more prone to delamination. In addition to strength, the effects of stitching on stiffness and damping properties are also investigated. In some of the applications that laminated composite materials are used for, knowledge of the resonant frequencies and damping properties are necessary in designing to avoid failure under excessive vibration. Another aspect of using composite materials for structural purposes is to consider the change in modal parameters given that, some form of damage has already occurred. With the difficulty in predicting shift in properties, analytical modelling proves even more challenging and warrants an experimental approach for dynamic characterization.

Experimental investigations by Mouritz et al. [6] to determine the effects of through-thickness stitching on in-plane properties of fiber-reinforced polymer composites found contradictions regarding the damage-resistance scaling in proportion to stitching. Mouritz [7] also conducted experiments on ballistic and explosive impacts on stitched composites which

revealed the stitching heavily improving damage resistance against explosive effects but very little against ballistic impact.

Arbaoui et al. [5] have shown through experimentation what effects the stitches have on composite dynamic properties. Their tests conducted on 2-D and 3-D woven E-glass/Vinyl Ester composites reveal some factors that the stitching have on the compression dynamic modulus of the material. First, the compression dynamic modulus has greater values along the stitch direction compared to the normal to the stitch direction. Second is the marked difference between the failure modes of the 3-D and 2-D woven composite; with the former showing damage such as matrix/fiber failure, fiber pullout and delamination etc. in the stitch direction and shear bending in the direction normal to stitching, with the latter undergoing matrix cracks and delamination to failure.

In 1976, Gibson et al. [8] attempted to establish a model analytically and subsequently, validate it experimentally for the internal damping and stiffness properties of E-glass/Epoxy beams under flexural vibration. Similar to what Arbaoui et al. [5] had found, Gibson et al. also discovered that strain amplitudes dictated the response of the dynamic modulus only beyond a certain threshold namely, the fracture strain of the ply. Material damage causes an increase in damping while reducing stiffness. Gibson [9] listed out all the methodologies of determination and evaluation of dynamic mechanical behavior of composite materials both experimentally and analytically. He explored the causes of the basic properties of composites determined theoretically differing from the experimental values and details the significance of numerical techniques in determining these properties [10]. Hwang and Gibson [11] conducted numerous experiments to illustrate the effects of the fiber/matrix interphase region on damping of composites and to build micro-mechanical models. Their research yielded the conclusion that

damping resulting from in-plane shear was more dependent on interphase size compared to other orientations.

Suarez et al. [12] developed fast techniques to measure damping without compromising accuracy and influence of ambient environment. Their comparative analysis of two different techniques came up with the conclusion that the impulse-frequency response technique of vibration analysis was better than the random technique. Mantena et al. [13 - 19] conducted a series of both low velocity impact tests as well as dynamic mechanical analysis on various types of composite laminates. Their work illustrates the determination of dynamic moduli of composites through non-destructive vibration testing methods and extends to the testing of different pultruded and sandwich composites along with the effects of temperature [13], adhesives [14] and environmental effects on their properties. These include axial and flexural configurations [15][16] as well as torsional [17][18]. Low-velocity impact response and vibration response of glass-resin composites [19] have also been discussed in their studies.

Li et al. [20] determined elastic properties for both stitched and un-stitched composite plates from their dynamic behavior which is otherwise not accessible through conventional mechanical testing methods. They claim to have been the first to try this method on a stitched composite plate, particularly the type with stitches dispersed in a heterogenous fashion and had identified over 20 mode shapes with average error percentage of only around 1.15%.

Moslehy [21] states the methods and details involved in conducting modal analysis using a loudspeaker although it has its limitations of not having the excitation concentrated to a point of interest. Numerous other contactless methods for determining elastic properties of composites have been developed and tested to obtain reasonable results [22-25].

Abrate [26-29] made a comprehensive review on the impact response of laminated

composites. The author subdivided damage from impact on laminated composites into fiber breakage, matrix cracking and delamination. Abrate & Schoeppner [30] validated the existence of a delamination threshold under low-velocity impact loading. Damage caused by impact to laminated composites are governed by several factors but as would be expected of a more homogenous material, Wyrick and Adams [31] showed that damage to carbon/epoxy laminates was highest below the point of impact and reduced in intensity with distance from the impact point. The damage amount was proportional to the impact energy, but the larger portion of damage was observed to be at the bottom ply.

Hosur et al. [32] conducted numerous tests on stitched and un-stitched composites, particularly S2-Glass/SC-15 Epoxy composites. These tests include high-velocity impact tests [32], low-velocity impact (single and repeated) [33][34], ballistic impact [35] etc. Their low-velocity impact tests show that woven fabric composites have less delamination and more of a localized damage from impact loading and that stitching improves mitigating damage when applied properly. A cylindrical spread of damage is observed for the stitched laminates while the un-stitched ones exhibit a more conical spread. Their work also revealed an efficient stitching dimension for the material in question in terms of impact performance.

Kang and Lee [36] from their experiments on varied composites have shown that stitching indeed improves energy absorption. However, their studies have also pointed out a key factor which is the development of localized stress concentration resulting from the needles used to sew in the stitches. To this, they proposed an optimum stitching density to accommodate damage mitigation without compromising risk of stress concentration. The effects and advantages of stitching in damage tolerance are also elaborated by Pelstring and Madan [37] who also pointed that low-velocity impact can be considered as one of the biggest causes of delamination. Stitches

can also delay the initiation of debonding in lap joints as shown by the studies of Glaessgen et al. [38].

Liu [39] conducted low velocity impact tests on epoxy matrix composites with several types of fiber reinforcement. These experiments investigated the effects and degree of influence of various factors on the delamination phenomenon which in turn is directly dependent on the inter-laminar strengths and stress levels. Factors ranging from matrix toughness, fiber-matrix bond, stitching, stacking sequence, elastic constants to lamina thickness, fiber angle etc. affecting interlaminar strength are involved in their tests. Aside from these factors, Dransfield [40] examined the micromechanisms of stitched composites and detailed the advantages and disadvantages of stitching on the occurrence of delamination, with an optimal combination between stitching and fabrication techniques to increase delamination resistance.

Damage detection is another point of concern in terms of laminated composites, especially internal delamination that may not be apparent to the eye. Among different techniques investigated to determine the damage primarily due to delamination such as using vibration [41-44], lamb waves [45][46] and electric potential [47]; vibration methods have been the most widely used ones.

Glass & Patterson, [48] described one of the earliest theoretical and experimental studies of shock tube flows. In another study by Aune et. al. [49], a shock tube setup is outlined in detail to replicate an unconfined far-field air blast that exhibited conformation to the idealized shock tube theory as well as simplified numerical simulations of generated wave patterns on structural applications which works as a good guideline on carrying out shock experiments.

Shukla et al. reported several works on shock loading of different metallic and composite materials. Detailed energy calculations based on both analytical and experimental observations

have been described by Wang and Shukla [50]. Although a good number of the studies done by Shukla et al. has been on sandwich composites [51-53], there are some works that focus on individual panels as well. Hebert et. al. [54] tested GFRPs made from E-Glass preforms combined with 3 different types of vinyl ester and urethane resin. Their experiments revealed that out of two composites having the same resin and same areal density, the ones with the finer glass structure showed better performance under shock loading.

Another study by LeBlanc et al. [55] investigates the application of coating (in this case, polyurea) on curved E-Glass/Vinyl Ester panels ( $0^\circ/90^\circ$  bi-axial layup) under simulated shock loading resulting from underwater explosions. Their findings state that an optimal coating thickness exists, preferably on the backside of the panel that can optimize the performance without bearing too much weight. LeBlanc et al. [56] further investigated under the same conditions, the same composites with 3 different layup constructions; namely, basic  $0^\circ/90^\circ$  bi-axial layup,  $0^\circ/90^\circ$  bi-axial layup with a glass veil between plies and  $0^\circ/90^\circ$  bi-axial layup with a polyurea coating on the back face of the panel. This study not only affirmed the findings of the study mentioned previously where the use of coating improved the performance; but in addition, showed that the insertion of glass veils actually weakened the panels.

The current paper deals with experimentally obtaining the dynamic modulus and damping from vibration tests, energy absorption due to low-velocity impact and the shock response of E- Glass/Vinyl Ester and S-Glass/Vinyl Ester of unstitched/stitched composites in various configurations. A comparative study of the obtained test data is made to observe the effects of stitching on said composites. While the modal properties (dynamic modulus and damping) are obtained by applying conventional formulae to the experimentation datasets, the impact properties are obtained directly from the associated experimental setup. In addition,

fracture energy calculation is carried out based on a model of penetration provided by Dorey [57]. While there have been similar experimentations conducted on these types of composite materials, this study provides a comparative picture of how stitching plays a role on these two FRPs with varying strength and stiffness properties.

### **1.3 Objective and Scope of the Study**

The objective of this study is to characterize the dynamic and energy absorption properties of E- and S- Glass/Vinyl Ester composites, with and without through thickness stitching. These stitched composites may be used as faceplates in sandwich structures with candidate foam core materials. This study is undertaken under a grant from ERDC, Vicksburg, Mississippi to develop a new class of materials with better blast, shock and impact resistance without compromising weight for military applications.

#### **1.3.1 Dynamic Properties**

The spectrum analyzer has been used to characterize the dynamic properties of the stitched/unstitched samples. It is a commonly used device in determining the storage modulus, loss factor, damping properties etc. of viscoelastic materials. It records and outputs obtained raw data from specimen subjected to oscillatory load as a desired transfer function. For this study, cantilever beam samples were subjected to flexural vibration to obtain storage modulus, damping and loss properties.

### **1.3.2 Low-velocity Impact**

Drop-weight low-velocity impact tests were conducted in order to obtain material response under low strain rate in flexural mode. Punch-shear test was used to characterize energy absorption properties for different stitched/unstitched specimen.

### **1.3.3 Shock Tube**

Circular samples were subjected to blast loading in a shock tube which is used to characterize material at medium strain rates. 3D DIC method was employed to obtain center point displacement, acceleration and energy absorption.

## CHAPTER II

### MATERIALS

#### 2.1 Material Used

E-Glass and S-Glass woven fabrics with vinyl ester resin were used to fabricate composite panels consisting of a plain weave and with two parts (base and MEKP catalyst, using 1.25% of catalyst). Each panel contained 20 plies of 304.8 mm x 304.8 mm (12 inch x 12 inch). Panels were fabricated to be square in shape utilizing vacuum infusion process to yield a typical 35 - 40% fiber volume fraction. The stitching was done so as to create cross-stitches with a gap of 50.8 mm (2 inch) in both in-plane directions and through the thickness in Z-direction with a loop stitch of 10 mm (0.5 inch) width. These composite panels were evaluated for application in lightweight sandwich structures as part of a funded research program. They were manufactured at and supplied by The Mississippi State University. Brief specifications of the panels are as follows:

- a) Un-stitched and Stitched S-Glass/Vinyl Ester Woven Composite Panels (Provided by ERDC, Vicksburg).

Set of 3 stitched and 3 un-stitched S-glass/vinyl ester woven composite panels, with six panels having 50.8 mm spaced horizontal and vertical through thickness stitching as shown in **Figure 3. Table 1** lists the dimensional properties of the panels with corresponding thicknesses.

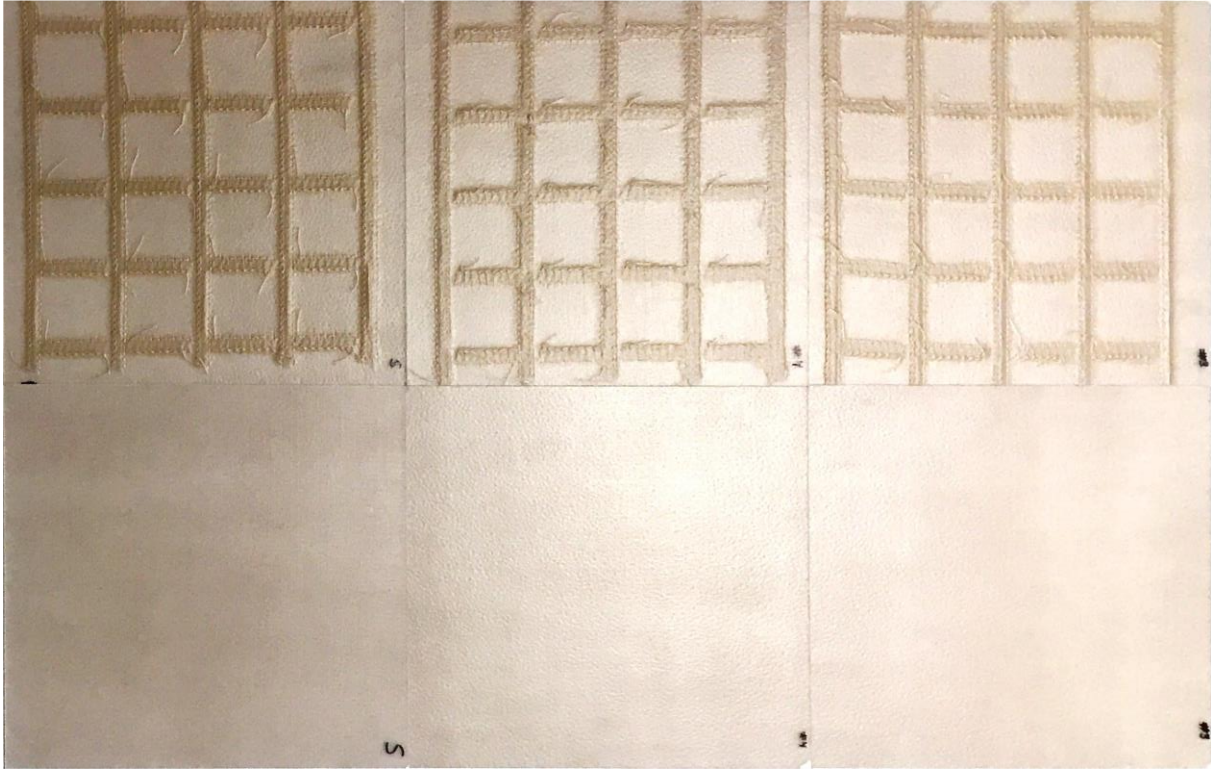


**Figure 3.** 3 stitched and 3 unstitched S-glass/vinyl ester woven composite panels (Courtesy: ERDC, Vicksburg)

**Table 1:** S-Glass/Vinyl Ester woven composite panels

Panel label	Stitched		Un-Stitched	
	Dimensions (mm)	Mass Density (kg/m <sup>3</sup> )	Dimensions (mm)	Mass Density (kg/m <sup>3</sup> )
#3	304.8 x 304.8 x 1.5	1481.8	304.8 x 304.8 x 1.3	1622.6
#4	304.8 x 304.8 x 1.5	1481.8	304.8 x 304.8 x 1.4	1602.8
#S	304.8 x 304.8 x 1.6	1448.8	304.8 x 304.8 x 1.4	1630.4

b) Un-stitched and Stitched E-Glass/Vinyl Ester Woven Composite Panels (Provided by ERDC, Vicksburg).

Set of 3 stitched and 3 un-stitched E-glass/vinyl ester woven composite panels, with six panels having 50.8 mm spaced horizontal and vertical through thickness stitching as shown in **Figure 4**. **Table 2** lists the dimensional properties of the panels with corresponding thicknesses.

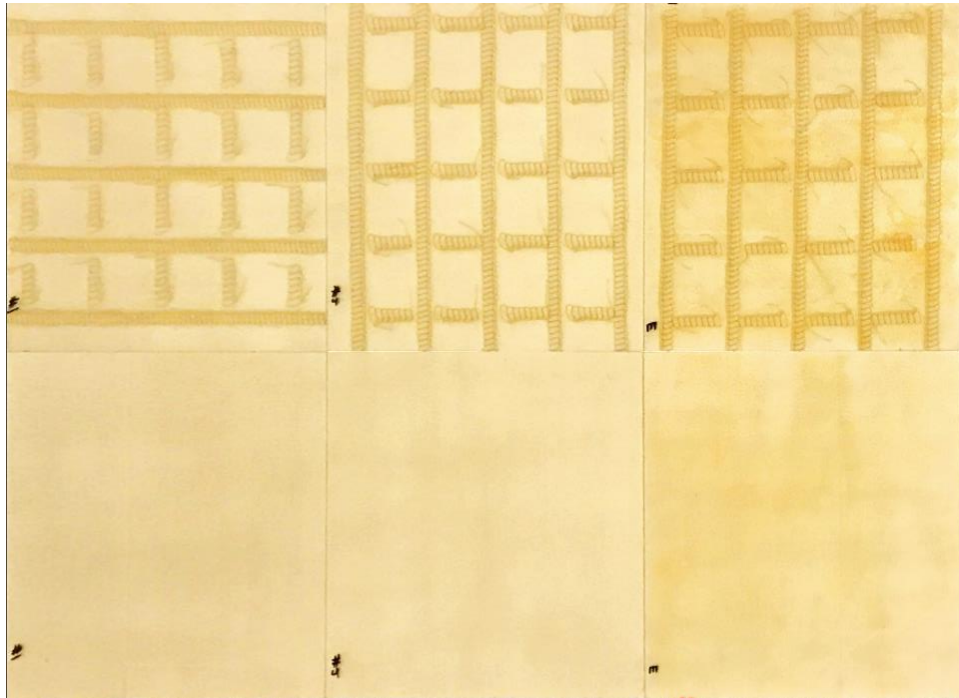


**Figure 4.** 3 stitched and 3 unstitched E-glass/vinyl ester woven composite panels

(Courtesy: ERDC, Vicksburg)

**Table 2:** E-Glass/Vinyl Ester woven composite panels

Panel label	Stitched		Un-Stitched	
	Dimensions (mm)	Mass Density (kg/m <sup>3</sup> )	Dimensions (mm)	Mass Density (kg/m <sup>3</sup> )
#1	304.8 x 304.8 x 1.55	1472.23	304.8 x 304.8 x 1.38	1622.39
#2	304.8 x 304.8 x 1.53	1491.47	304.8 x 304.8 x 1.37	1618.51
#E	304.8 x 304.8 x 1.55	1472.23	304.8 x 304.8 x 1.37	1602.80

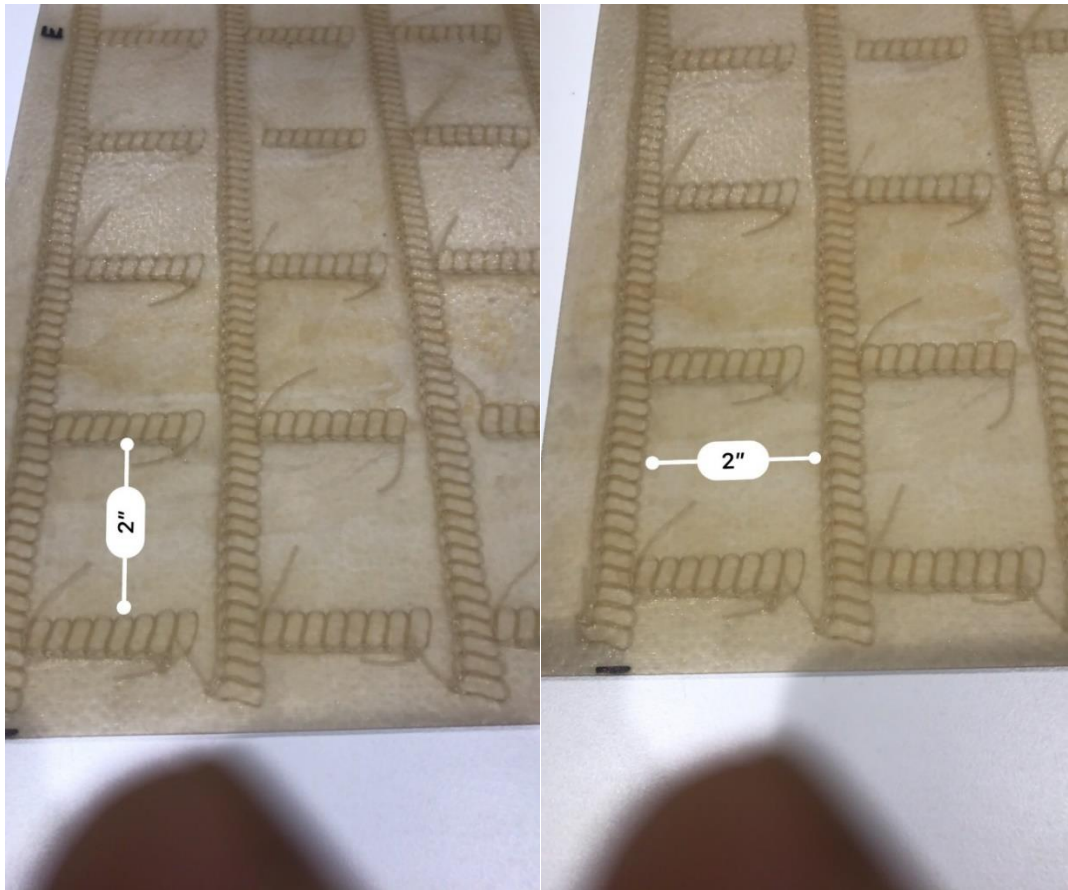


**Figure 5.** Loop stitch (0.5 inch width) with a gap of 2 inch in-plane directions.

**Figure 5** shows the gap between each line of stitching on the panel surface. A point to be noted as seen in Tables 1 and 2, is that the density appears to be less for the stitched panels compared to the unstitched ones. This is due to the fact that for the stitched specimens, the stitching occupies equivalent volume within the panels as the composite resins in the unstitched panels. Since the stitches themselves consist of less density than the polymer matrix of a 35 – 40% fiber volume fraction composite, the overall density of the stitched composite appeared to be less than the actual density of the otherwise unstitched composite. It has been observed that the stitches constitute about 25% of the total volume of each panel while the rest is occupied by the woven fiber reinforced polymer matrix. Also, fluctuations over the stitched and unstitched region had to be considered for arriving at an average sample thickness, needed for computing the density and dynamic flexural modulus theoretically.

To accommodate for varying thickness over stitched and unstitched portions, weighted average of measured thicknesses was calculated considering 75% of the beam’s total volume as unstitched portion (fiber + matrix) and 25% with stitches to account for the fact that stitches occupy a fraction of the total volume. This estimation is obtained by using Equation (1) where  $t$  denotes thickness and the corresponding subscripts according to location.

$$t = 75\% t_{unstitched} + 25\% t_{stitched} \quad (1)$$

As seen in the previous tables, the panels were labeled as  $I$ ,  $2$  and  $E$  for E-glass while  $3$ ,  $4$  and  $S$  for the S-Glass by the manufacturer/supplier. For this study, one specimen for each type of experiment from each panel were taken and are labeled in the format of ‘ $MZRn$ ’; where,

*M* denotes Fiber Glass (E- or S-Glass)

*Z* denotes 3-D reinforcement (Stitched, S / Unstitched, U)

*R* denotes Polymer resin (Vinyl Ester)

*n* denotes panel number (1, 2, 3, 4, E or S)

## 2.2 Specimen Preparation

Samples of required dimensions were cut using CNC laser cutting machine and kept inside plastic bags before and after each round of experimentation to prevent moisture absorption and/or foreign particle accumulation. For the vibration analysis, specimens with lengths of 254 mm (10 inch) and 25.4 mm (1 inch) width were cut from the source panels. Each specimen was clamped with 127 mm (5 inch) free length suspended in cantilever configuration.

For the low-velocity impact test, square specimens of 101.6 mm x 101.6 mm (4 x 4 inch) dimensions were cut from each respective panel. The average thickness was around 1.5 mm as stated earlier in Tables 1 and 2. For shock tube experiments, specimens were made circular with a diameter of 127 mm (5 inch). The thickness remained the same corresponding to each panel from **Table 1** and **2**.

## CHAPTER III

### EXPERIMENTAL PROCEDURE

#### **3.1 Vibration Experimental Procedure**

Experimental modal analysis is carried out to investigate and validate the stability of structures. Modal parameters of a structure are frequency, damping and mode shapes that are functions of its physical properties e.g., frequency is directly proportional to the stiffness and inversely proportional to mass.

There are two commonly used types of excitation methods for experimental modal analysis: hammer and shaker excitation. The former is used in this experiment to determine the modal properties. Dynamic and damping properties can be evaluated experimentally using either time or frequency domain characterizations. For time domain analysis, oscilloscope can be used whereas for the frequency domain analysis, signal analyzers are used. The signal or spectrum analyzer, basically uses Fourier transform subroutine to transform the time domain response into frequency domain function. The response may be given in terms of displacement, velocity, or acceleration. A frequency response function or FRF is a transfer function, defined as the ratio between the displacement, velocity or acceleration response to the input force expressed as a function of frequency. The applied force and the response of the system both are measured simultaneously. The measured time data is then transformed from the time domain to frequency domain using Fast Fourier Transform (FFT) algorithm available in signal processing analyzer.

Hammer excitation was employed to determine the modal parameters of the composite specimens. In this method, cantilever beam specimens are subjected to flexural mode of vibration. The first three natural frequencies are obtained experimentally of which, the first natural frequency has been used for determining the flexural stiffness and the damping constant. The results are also validated by checking the coherence function.

The input and output signal source are connected to a spectrum analyzer through a signal amplifier. The input signal source is the hammer, and the output source is an accelerometer mounted on the clamped cantilever beam specimen. The hammer has a force transducer at its tip to measure the applied load. The modal parameters can be determined from a set of frequency response measurements between a reference point and several measurement points. Such a measurement point is called a degree of freedom. The modal frequencies and damping can be found from all frequency response measurements on the structure except those for which the excitation or response measurement is in a nodal position where the displacement is zero.

Vibration response of the composite specimens has been investigated in the cantilever beam flexural configuration. This setup is used to determine the dynamic modulus and loss factor (measure of damping) of the E-glass and S- glass /Vinyl ester composite specimens. Equation of motion for a beam vibrating in flexure [58] is given as:

$$EI \frac{\partial^4 W}{\partial X^4} + \rho A \frac{\partial^2 W}{\partial t^2} = 0 \quad (2)$$

Where,  $E$  = Flexural Modulus of elasticity

$I$  = Area moment of inertia of beam cross-section

$W$  = Displacement of neutral axis

$\rho$  = Beam mass density

$A$  = Beam cross-sectional area

$t$  = time

Using separation of variables approach, the eigenvalue solution gives:

$$\lambda = \sqrt{\frac{\omega_n^2 \rho A}{EI}} \quad \text{or} \quad \omega_n = \frac{(\lambda_n L)^2}{L^2} \sqrt{\frac{EI}{\rho A}} \quad (3)$$

Here,  $\lambda_n$  = Eigen value of the nth mode

$\omega_n$  = natural frequency of the nth mode

For a fixed-free cantilever beam boundary condition are:

1st mode:  $\lambda_1 L = 1.875$

2nd mode:  $\lambda_2 L = 4.694$

3rd mode:  $\lambda_3 L = 7.855$

For dynamic conditions, Young's modulus can be written in complex terms as:

$$E^* = E' + iE'' \quad (4)$$

Storage modulus,  $E'$  represents the elastic (real part) component of the complex modulus. This is the part of the modulus that is proportional to the stored energy that is recovered instantaneously. The loss modulus ( $E''$ ) represents the part of the modulus that is dissipative and consequently non-recoverable. Loss factor (damping) is given by:

$$\eta = \frac{E''}{E'} = \tan \delta = 2\zeta \quad (5)$$

Each of the frequencies produced from the signal analyzer correspond to the peaks along the horizontal (frequency) axis. Damping can also be found from frequency do-main data with the half-power bandwidth method which was foregone in the case of this experiment. Using the frequency domain data obtained directly from the spectrum analyzer the loss factor, storage modulus and loss modulus can be computed by using the following equations:

$$\eta = 2\zeta = \frac{\omega_2 - \omega_1}{\omega_n} = \frac{f_2 - f_1}{f_n} \quad (6)$$

$$E' = \frac{4\pi^2 f_n^2 L^4 \rho A}{(\lambda_n L)^4 I} \quad (7)$$

$$E'' = \eta E' = \tan\delta E' \quad (8)$$

In the hammer excitation method, cantilever beam specimens are subjected to flexural mode of vibration. Two representative specimens tested from E- and S-Glass/Vinyl Ester samples are shown in **Figure 6**.



(a)



(b)

**Figure 6.** Specimens for vibration analysis cut from (a) Stitched, and (b) Unstitched E-Glass/Vinyl Ester composite panels

The step-by-step procedure carried out in order to obtain the flexural modulus and damping are described below with associated illustrations:

First, proper connections are setup which essentially involves connecting the input and output signal sources to a spectrum analyzer through a signal amplifier (Shown in **Figure 7**). In this case, the input signal is obtained from hammer excitation and the output response from an accelerometer.



(a)



(b)

**Figure 7:** (a) Spectrum Analyzer (b) Signal Amplifier

Both input and output signals are connected to the spectrum analyzer through a signal amplifier. The beam specimen is clamped with the help of a vice firmly and the accelerometer is attached to the designated position (e.g., as shown in **Figure 8**).

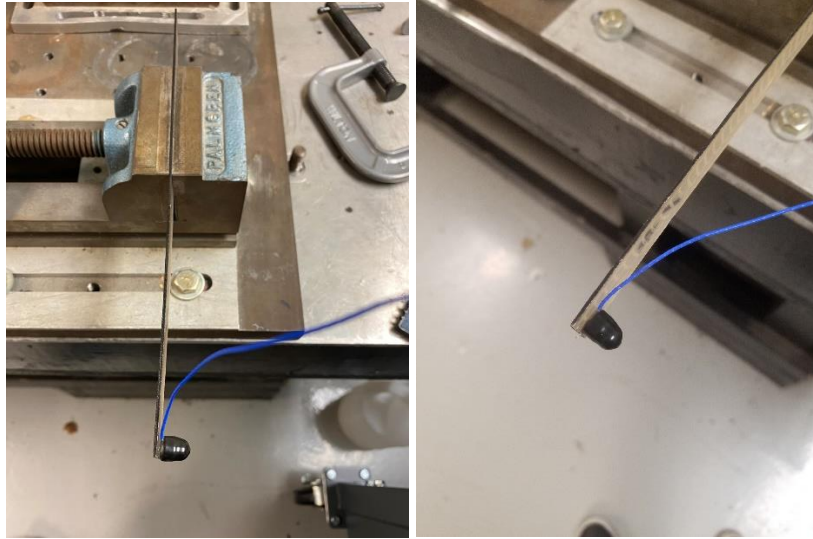


**Figure 8.** Mounting the sample and attaching the accelerometer on the specimen

The system is calibrated to achieve reasonable FRF traces for the beam vibration. In this case a range of 800 Hz is chosen in order to capture the range of the first three natural frequencies. After that, the beam is tapped at a position closest to the fixed end with the accelerometer attached at the free end till a clean FRF magnitude plot is obtained (as shown in **Figure 9**).



**Figure 9.** Tapping the specimen at the proper location in accordance with the desired FRF matrix element

An average of five readings are determined of the magnitude plots and the respective peaks for first three natural frequencies are identified. The amplitudes of the three natural frequencies in the FRF magnitude plot are saved through the interface of the analyzer. The range is reset to a smaller scale (e.g., around 50 Hz) and centered in on the first natural frequency for better resolution and visualization. These steps are repeated to determine a more precise value of the frequency. Using the navigation buttons on the interface panel of the analyzer, the value of damping constant, coherence plots etc. are determined to verify the integrity of the results obtained and record the necessary data accordingly.

### 3.2 Low-Velocity Impact Experimental Procedure

Impact tests are divided into two types: low and high velocity impact [19]. In the case of low-velocity impact, it is assumed to be a quasi-static process where the velocity is lower than 10 m/s and the effects of stress waves can be ignored.

A CEAST 9450 (Drop weight impact testing machine from Instron) setup was used to conduct low-velocity impact tests on 101.6 mm x 101.6 mm square specimens cut from the sample panels. The setup is shown in **Figure 10**. It utilizes a drop weight testing principle where damage on the specimen is experimentally obtained by puncturing the specimen using a narrow bar with a 20 mm hemispherical tip (or ‘tup’) that weighs 5.5 kg to facilitate penetration. The setup consists of a pneumatic system alongside a crosshead with an additional mass of 25 kg which travels vertically downwards along frictionless guide rails. Anti-rebound mechanisms is coupled to the system to ensure non-repeated, single impact. The impact energy can be manipulated by the mass being put on, the velocity of the crosshead, the drop height etc. All these parameters can be changed either physically or by ‘Bluehill<sup>®</sup> Impact’, a software that runs in conjunction with the setup in order to assist with testing, operating and recording data.

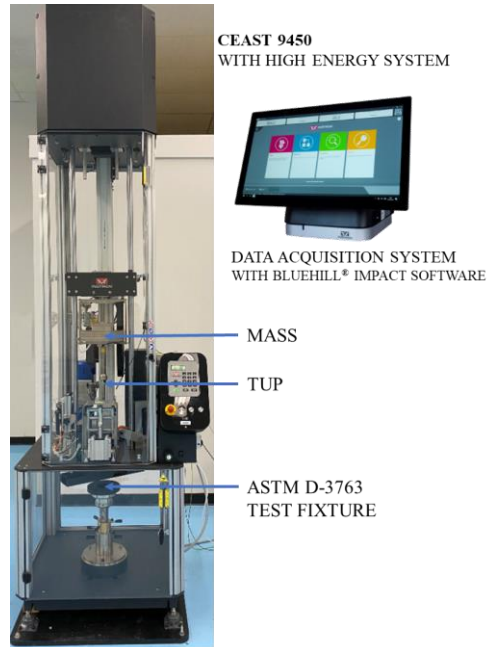


**Figure 10.** CEAST 9450 drop weight impact system with pneumatic assist and data acquisition system dashboard matrix

For the current study, specimens were subjected to punch shear loading with a steel tup at an impact velocity of 2.57 m/s and impact energy of 100.7 J. In accordance with the prescription of ASTM D3763 standard, the velocity slowdown was kept below 20% for all cases. A clamping fixture kept at 0.6 MPa uniform pressure ensures stability of the specimen during testing and creates a closed circular boundary condition on the impacted surface. The ‘Bluehill® Impact’ software records data at a sampling rate of 1 MHz and it is filtered through a 1360 Hz cut-off Butterworth low-pass filter.

### 3.3 Shock Tube Experimental Procedure

Shock tube experiment utilizes a highly energetic event where a shock wave is created by means of fluids (particularly gaseous in nature) kept at separate pressures and then the sudden release of the said fluid. This induces flow into the fluid as it begins to travel from the state of higher pressure to the lower pressure, converting energy following the Bernoulli's equation and satisfying the principles of conservation of mass and energy. This helps to determine strength characteristics for a particular piece of material from an engineering perspective. The schematic of a typical shock wave generation and propagation process is depicted in **Figure 11** [50] where a planar shock wave is used to apply load on a flat specimen at the end of a tube. This experimental setup where a planar incident shock front loads a flat panel can work as a model for evaluation of energy absorption and deflection. In the figure, a planar incident shock wave front is traveling from the left side to the right side through a shock tube (incident process). In front of the shock front, which is the right-side part inside the shock tube, the gas is undisturbed while the left side is the driver gas. The shock front travels to the end of the tube where the specimen is located and fixed with predetermined boundary conditions. There, the specimen undergoes shock loading and a reflected wave is generated which travels back in the opposite direction (reflected process). In this scenario, the gas in front of the reflected shock front will still remain as the driver gas but behind the shock front i.e., the right side of the tube will now have gas that has been disturbed by the reflected wave.  $U^+$  and  $U^-$  are the velocities of the incident and the reflected shock wave fronts, respectively. The state of the gas can be defined using the following physical parameters:  $p$ , the pressure;  $u$ , the particle velocity;  $c$ , the sound velocity;  $\rho$ , the density;  $\tau$ , the specific volume (i.e., volume per unit mass) and  $e$ , the specific internal energy.

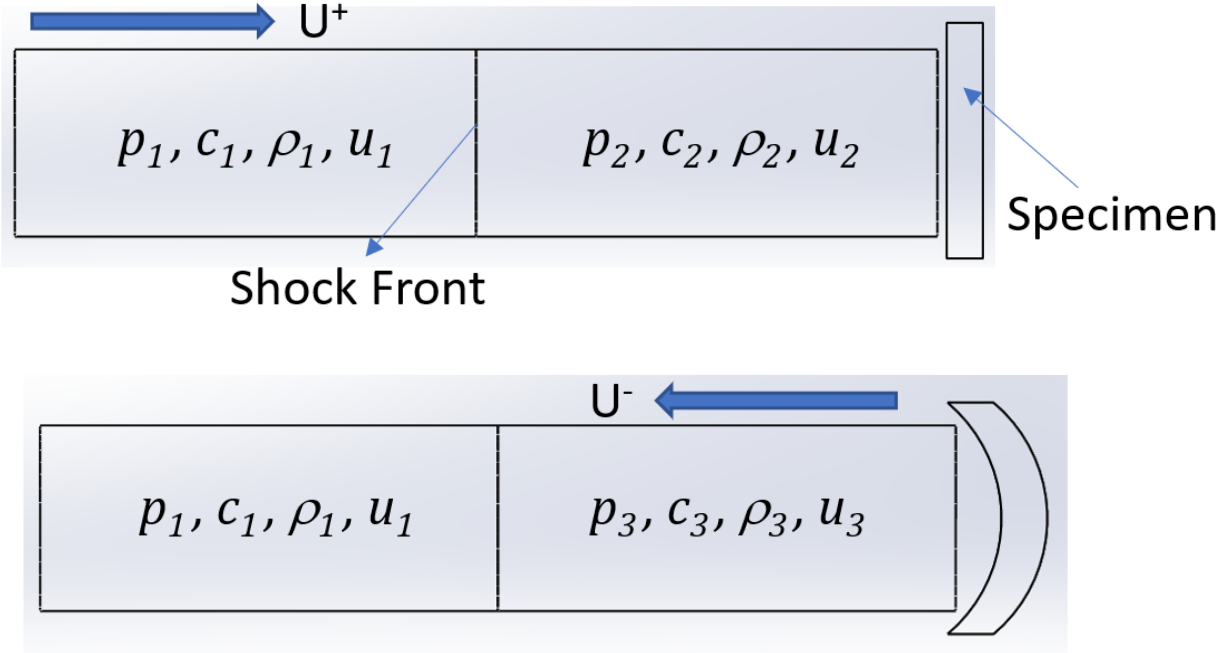


**Figure 11.** Schematic of the incident and reflected wavefront travelling through the shock tube

[51]

The states of the gases in the driver section are denoted by the subscripts 1 and the initial states of the undisturbed gases are denoted by the subscripts 2. Subscripts 3 represent the state of the gas after the reflected shock front has passed. Likewise, the energy stored in the gas located behind the incident shock front is defined as the incident energy and the for the one behind the reflected shock front will be reflected energy.

Following the shock theory covered by Wang and Shukla [51], if a gas has a pressure profile given by  $p(t)$  and it propagates inside a shock tube having a cross-sectional area of  $S$  and at a particle velocity of  $u(t)$ ; the internal, translational energy as well as the work done by the gas over an infinitesimal time span  $dt$  can be described by the following equations:

$$dE_{internal} = \frac{p(t) \cdot S \cdot |u(t)|}{\gamma - 1} dt \quad (9)$$

$$dE_{translational} = \frac{1}{2} * p(t) * S * |u(t)| * |u(t)|^2 dt = \frac{1}{2} * p(t) * S * |u(t)|^3 dt \quad (10)$$

$$dE_{work} = p(t) * S * |u(t)| dt \quad (11)$$

Where  $\gamma$  is the adiabatic exponent of gas.

For this study, the shock tube apparatus used was a variable pressure control shock tube (Srushti Engineering Innovations Ltd.) that has a high-speed valve to quickly release the compressed fluid. On the trigger end, the volume of fluid (which in this case is nitrogen) can be controlled and was set as such that, the initial pressure would be 4.2 MPa for the driving section. On the far end of the tube, circular specimens of 127 mm diameter were mounted between two circular flanges and bolted evenly on both sides to ensure that the shock front impacts the specimen normal to its surface. The flanges imposed a fixed boundary condition of 80mm diameter on the specimen surface and the area within this diameter is considered for measurements and inspection. Two Kulite HKS-HP-375-5000SG pressure transducers located 125mm apart from each other and the closest transducer to the specimen was a bit farther away from its surface, record the pressure data through a Kulite KSC-2 signal conditioning and amplification system. The maximum excitation and output voltage for the transducers were set to 5V with a 10 kHz filter. **Figure 12** shows the schematic of the necessary parts pertaining to the specimen mounting and image capturing.

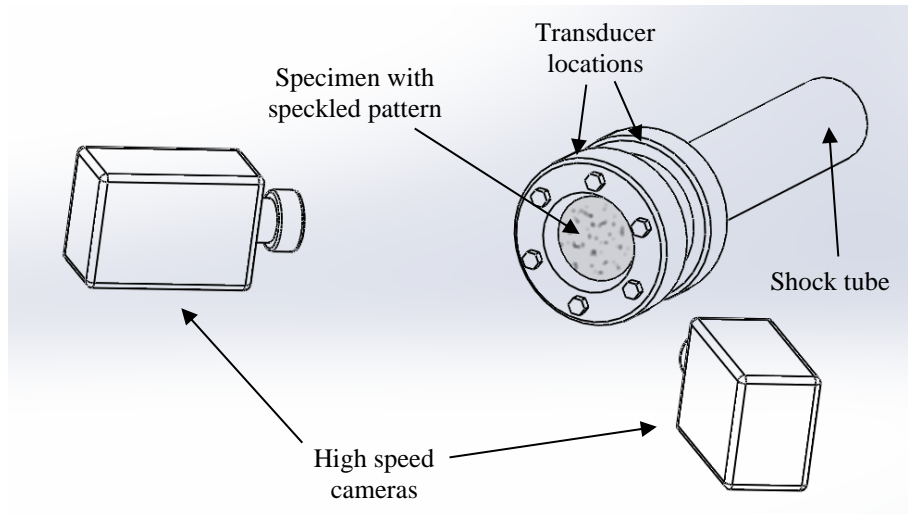


**Figure 12.** Schematic of specimen mounting using flanges and camera location

The cameras used for capturing deformation footage were Shimadzu HPV2 High Speed cameras with a capacity of up to a million frames/second. For this experiment, it captured the deformation footage at  $32 \mu\text{s}/\text{frames}$  and at a fixed resolution of  $312 \times 260$  pixels. These footages are later analyzed with the help of 'GOM Correlate' which is a 3D DIC analysis tool. The pressure profiles captured by the transducers are plotted directly by another software, Picoscope<sup>®</sup>

6.

CHAPTER IV  
RESULTS AND DISCUSSION

**4.1 Vibration Analysis**

Considering the thickness adjustment made according to Equation (1), the stitching in the composite specimens showed marked decrease in the resonant natural frequency and in turn, dynamic flexural modulus. But the loss factor barely showed much change with all specimens having an average of 0.02 loss factor ( $\eta$ ). The results from the tests are given in **Tables 3** and **4**.

**Table 3:** Frequency Domain Analysis Results of E-Glass/Vinyl Ester.

Sample	Avg. Experimental First Natural Frequency $f_n$ (Hz)	Avg. Damping Ratio $\zeta$	Avg. Loss Factor $\eta$	Avg. Flexural Modulus $E'$ (GPa)
EUV1	32.3	0.009	0.020	8.69
EUV2	29.8	0.010	0.020	7.92
EUVE	30.3	0.010	0.020	8.42
ESV1	34.3	0.012	0.025	10.65
ESV2	34.3	0.009	0.018	9.67
ESVE	33.9	0.012	0.025	9.26

**Table 4:** Frequency Domain Analysis Results of S-Glass/Vinyl Ester.

Sample	Avg.	Avg.	Avg. Loss	Avg.
	Experimental First Natural Frequency $f_n$ (Hz)	Damping Ratio $\zeta$	Factor $\eta$	Dynamic Flexural Modulus $E'$ (GPa)
SUV3	33.7	0.013	0.030	9.54
SUV4	33.7	0.012	0.020	9.49
SUVS	35.2	0.013	0.030	9.55
SSV3	37.6	0.009	0.020	12.49
SSV4	38.0	0.009	0.020	12.39
SSVS	37.1	0.009	0.020	13.52

**Figure 13** shows a comparative bar chart along with data scatter of dynamic flexural moduli and loss factors for stitched and unstitched E- and S-Glass/Vinyl Ester specimens from vibration experiments.

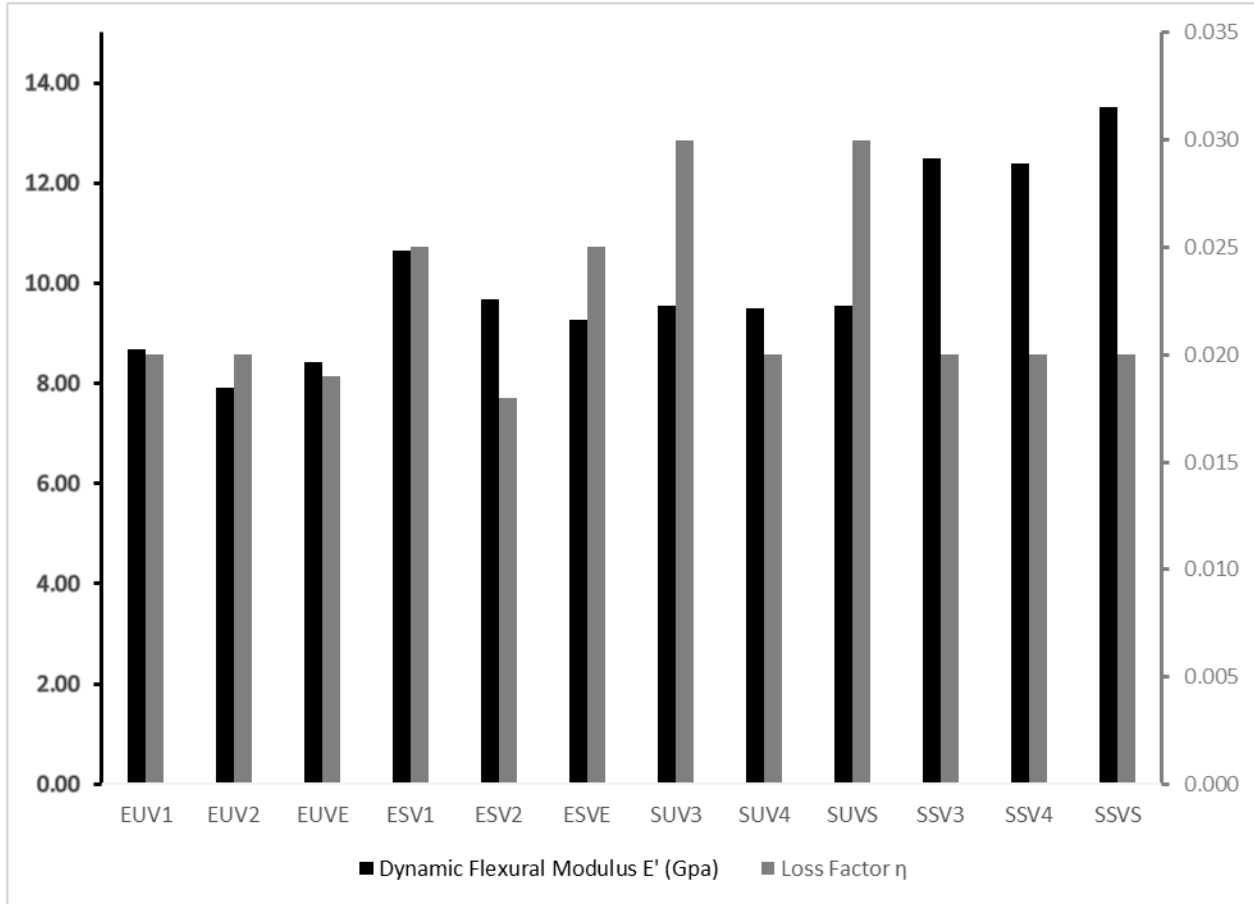


**Figure 13.** Dynamic Flexural Modulus ( $E'$ ) and Loss Factor

( $\eta$ ) for each unstitched and stitched E- and S- Glass/Vinyl Ester specimens from vibration experiments.

**Figure 14** shows a similar comparison but with all the specimens condensed to their specific category for the E- and S- Glass/Vinyl Ester Stitched/Unstitched samples.

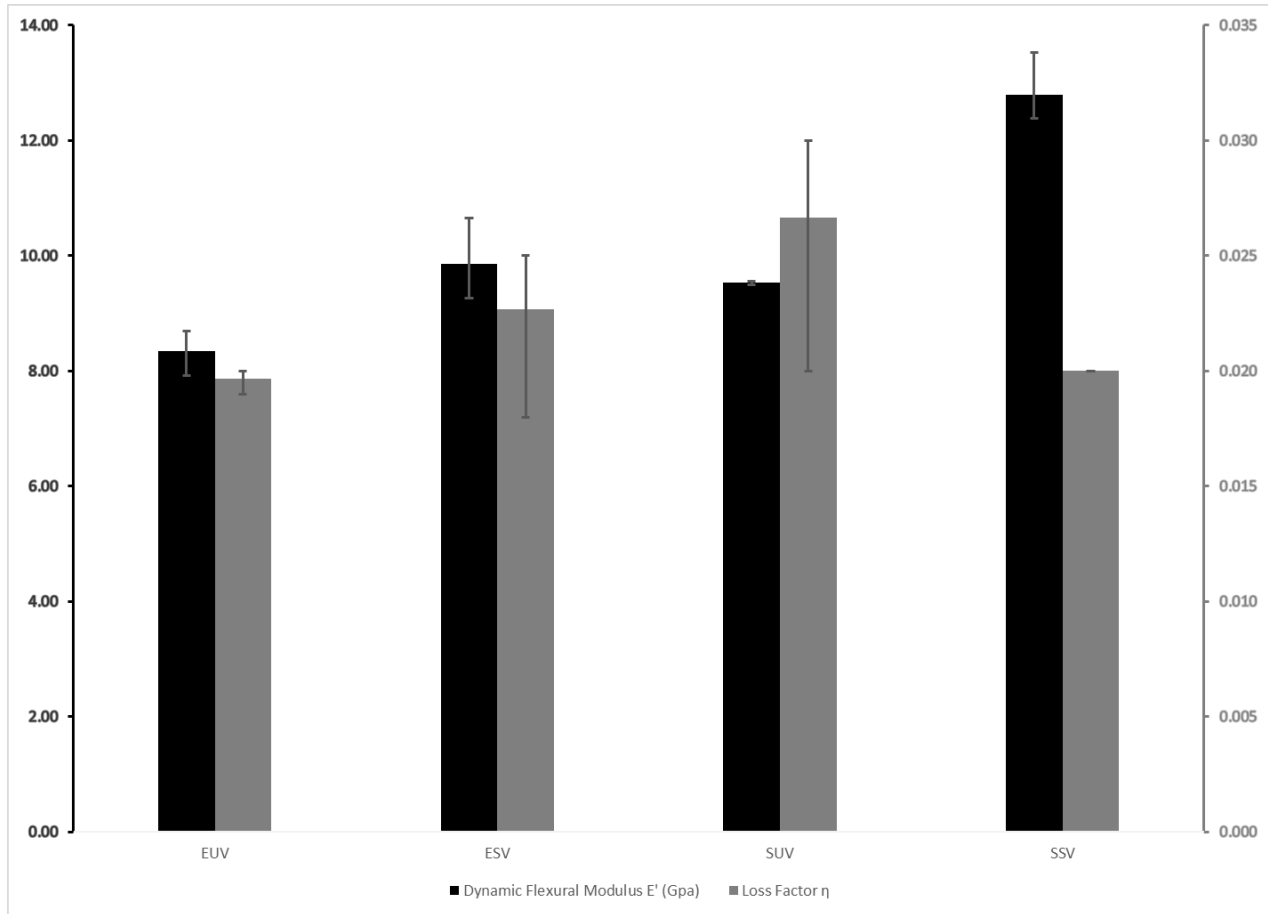


**Figure 14.** Dynamic Flexural Modulus ( $E'$ ) and Loss Factor ( $\eta$ ) for all types of specimens.

From **Table 3** and **4**, it is observed that the first resonant frequency for unstitched E-Glass/Vinyl Ester specimens is approximately 31 Hz whereas for stitched, it is approximately 34 Hz. In the case of S- Glass/Vinyl Ester specimens, the unstitched specimens first natural frequency of approximately 34 Hz and the stitched specimens had approximately 37 Hz. The stitching in both cases follow similar trends for the dynamic flexural modulus, increasing by roughly 13% and 8% respectively and it is likely that the higher stiffness within the stitching material itself induces increase in stiffness in the overall FRP composite. Another fact that conforms to other relevant studies in literature is the higher stiffness observed in the S- Glass

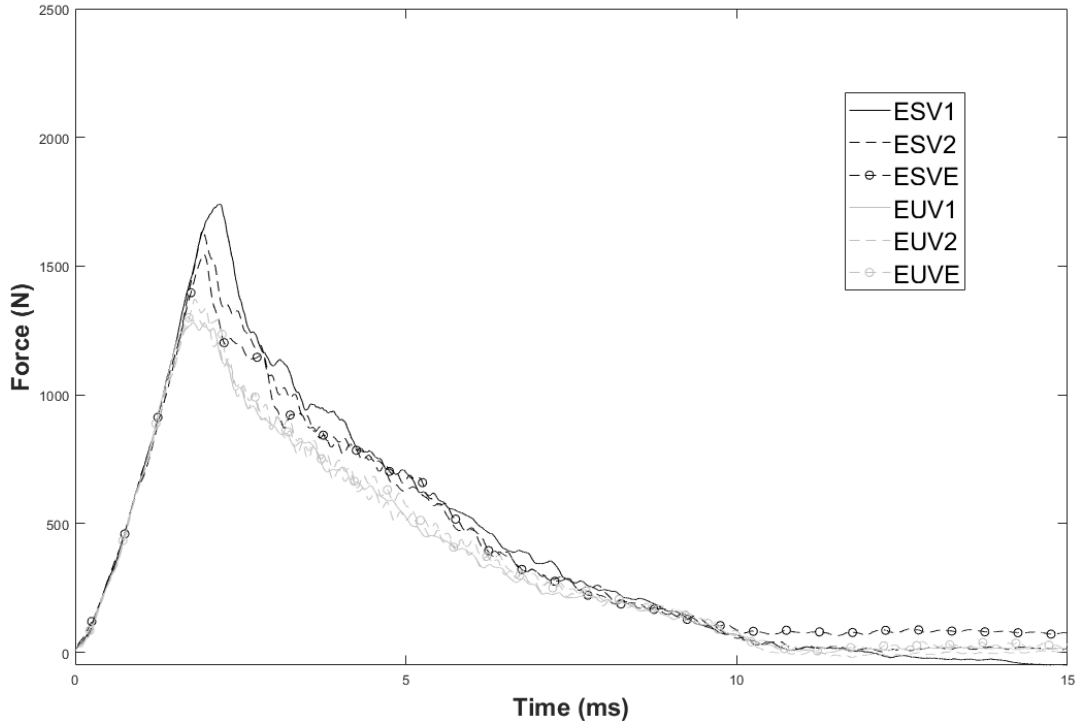
fiber reinforced specimens compared to E- Glass fiber reinforced ones. The stitching adds further to the higher value of stiffness although the damping properties remained unaffected.

## 4.2 Low-Velocity Impact Analysis

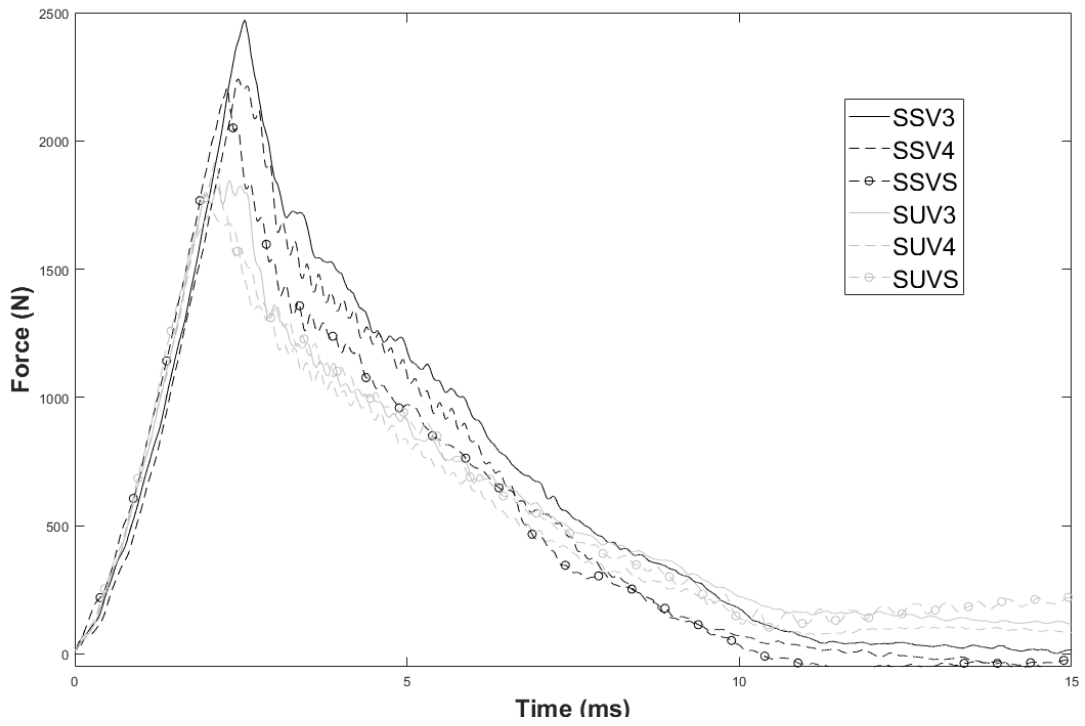
The low-velocity punch shear tests demonstrated distinct enhancement in properties resulting from stitching. This is also supported by the studies of Hosur et al. [32-35]. With the help of Bluehill® Impact software, the force-time history as well as deflection-time history can be obtained. The energy absorption can be computed with numerical integration of the load vs deflection plot following Equation (12).

$$E = \int_0^S F(s)ds \quad (12)$$

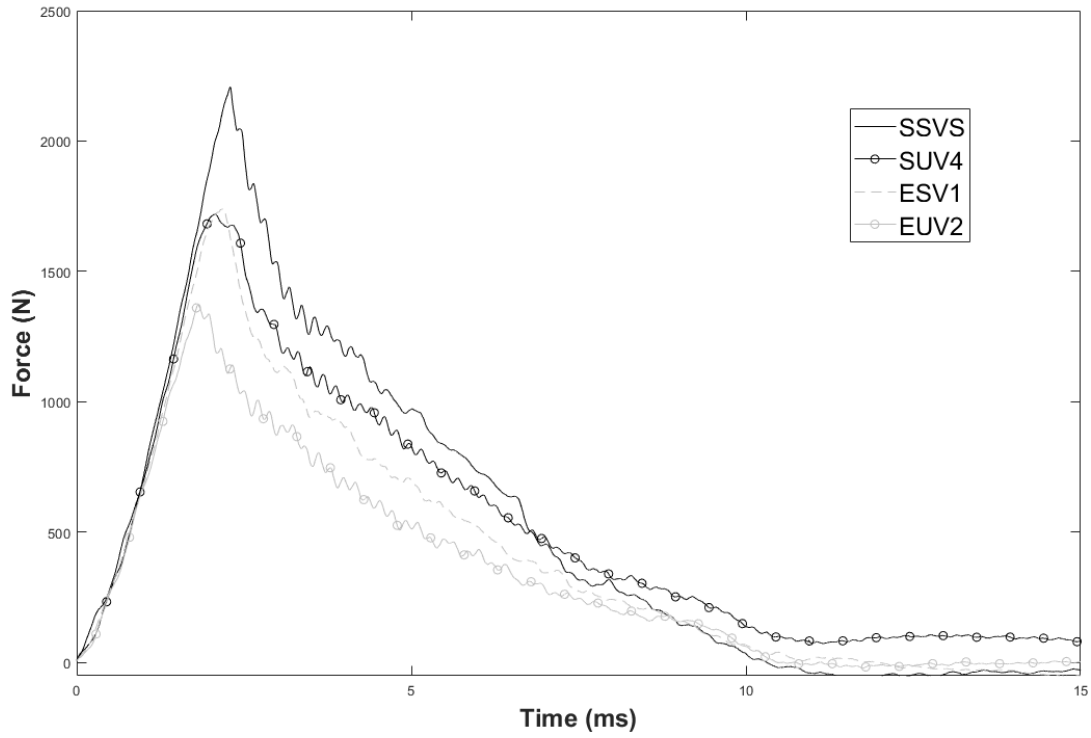
Analysis of load-time, load- deflection and load-deflection-energy curves reveal a particularly stepped linear pattern of increase in peak loads starting from unstitched E-Glass/Vinyl Ester specimens all the way up to S-Glass/Vinyl Ester, as shown in **Figures 15, 16, 17 and 18.**



(a)

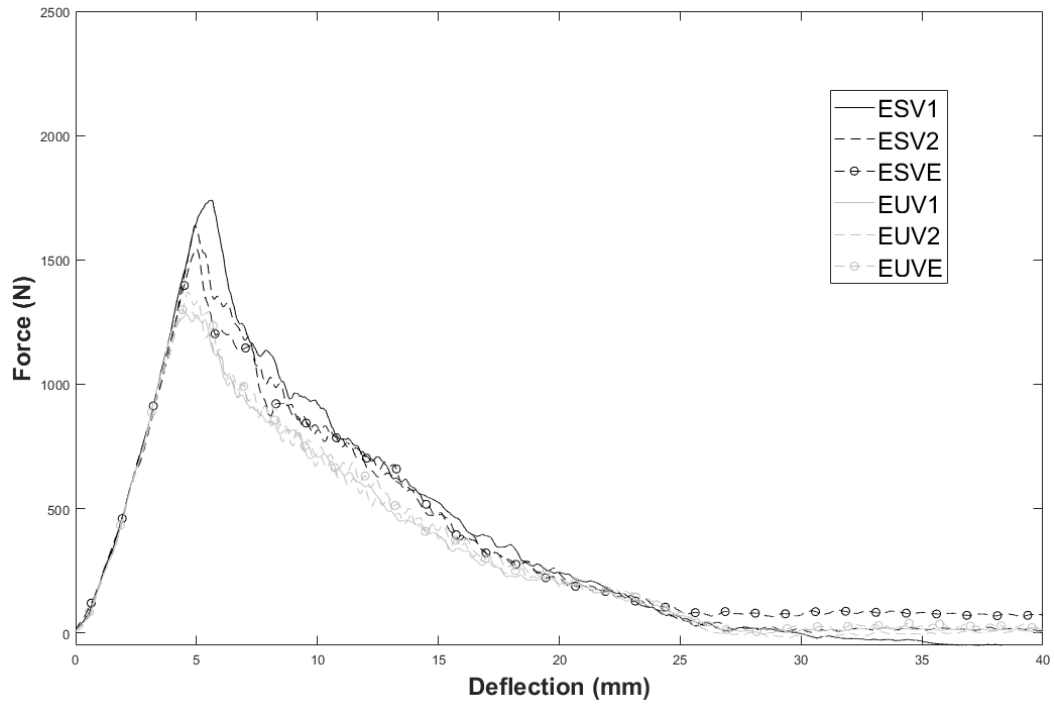


(b)

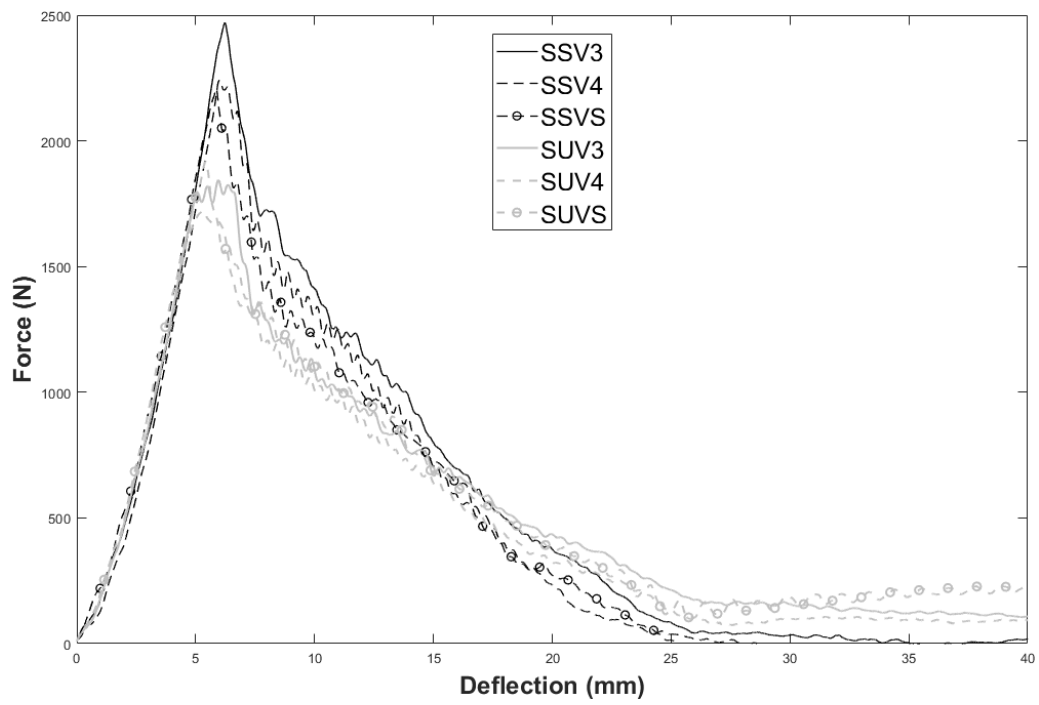


(c)

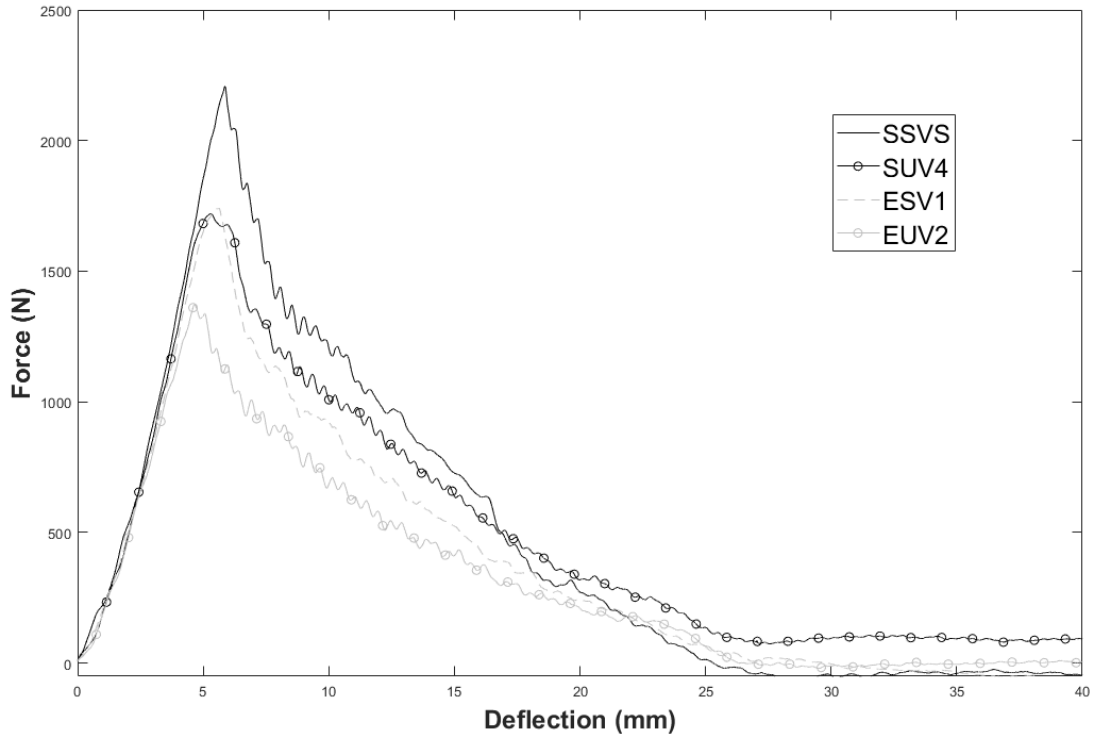
**Figure 15.** Comparison of Force vs Time plots for (a) E- Glass/Vinyl Ester (b) S- Glass/Vinyl Ester and (c) between representative specimens of E- and S- Glass/Vinyl Ester samples from low velocity punch-shear tests.



(a)

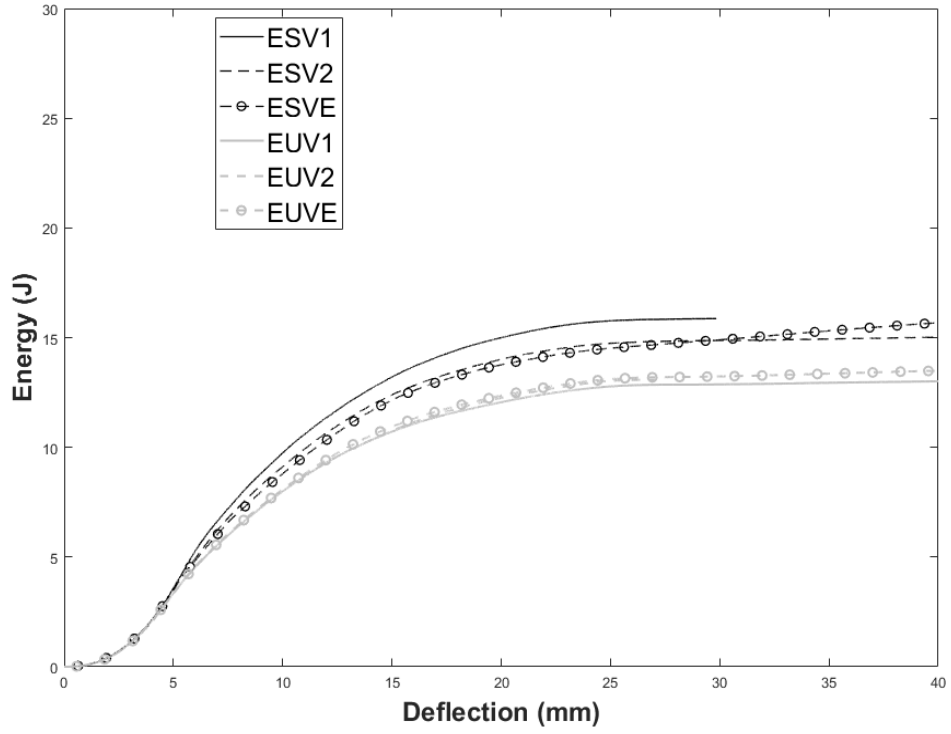


(b)

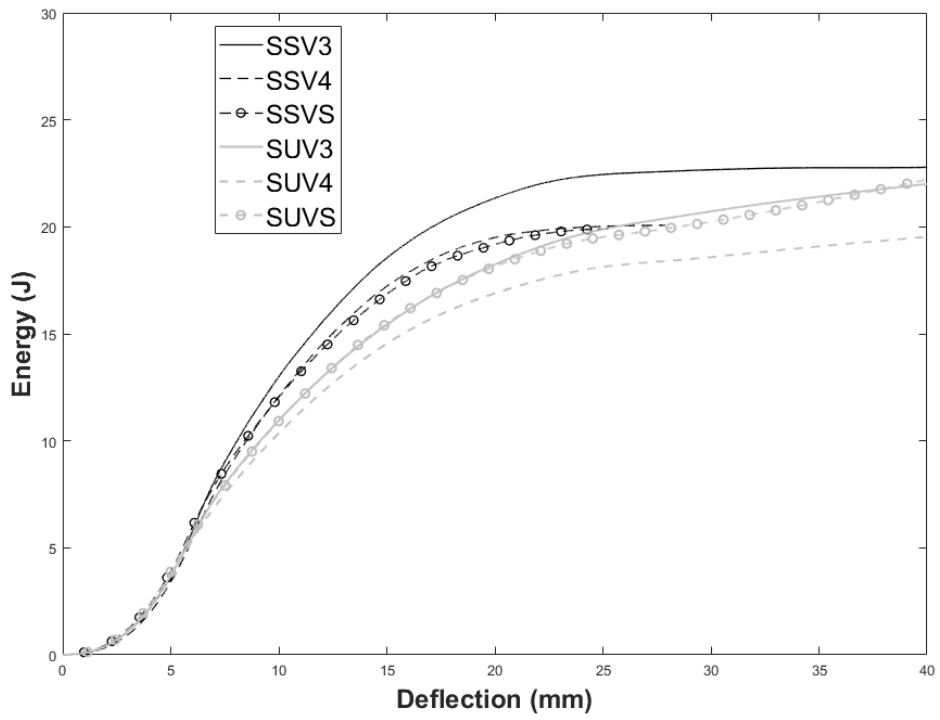


(c)

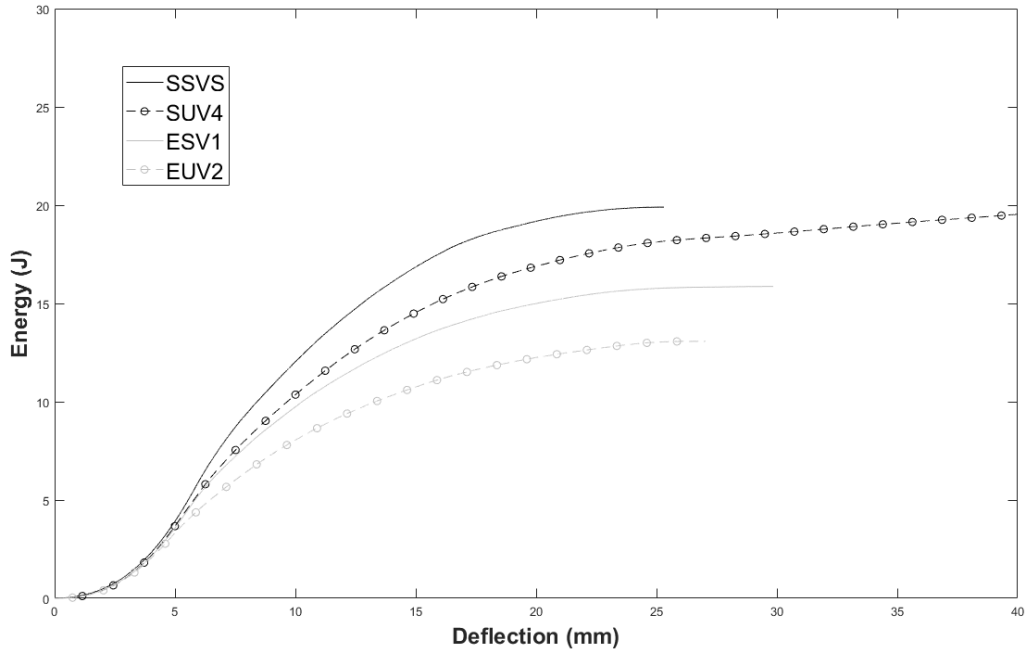
**Figure 16.** Comparison of Force vs Deflection plots for (a) E- Glass/Vinyl Ester (b) S- Glass/Vinyl Ester and (c) between representative specimens of E- and S- Glass/Vinyl Ester samples from low velocity punch- shear tests.



(a)



(b)



(c)

**Figure 17.** Comparison of Energy vs Deflection plots for (a) E- Glass/Vinyl Ester (b) S- Glass/Vinyl Ester and (c) between representative specimens of E- and S- Glass/Vinyl Ester samples from low velocity punch- shear tests.

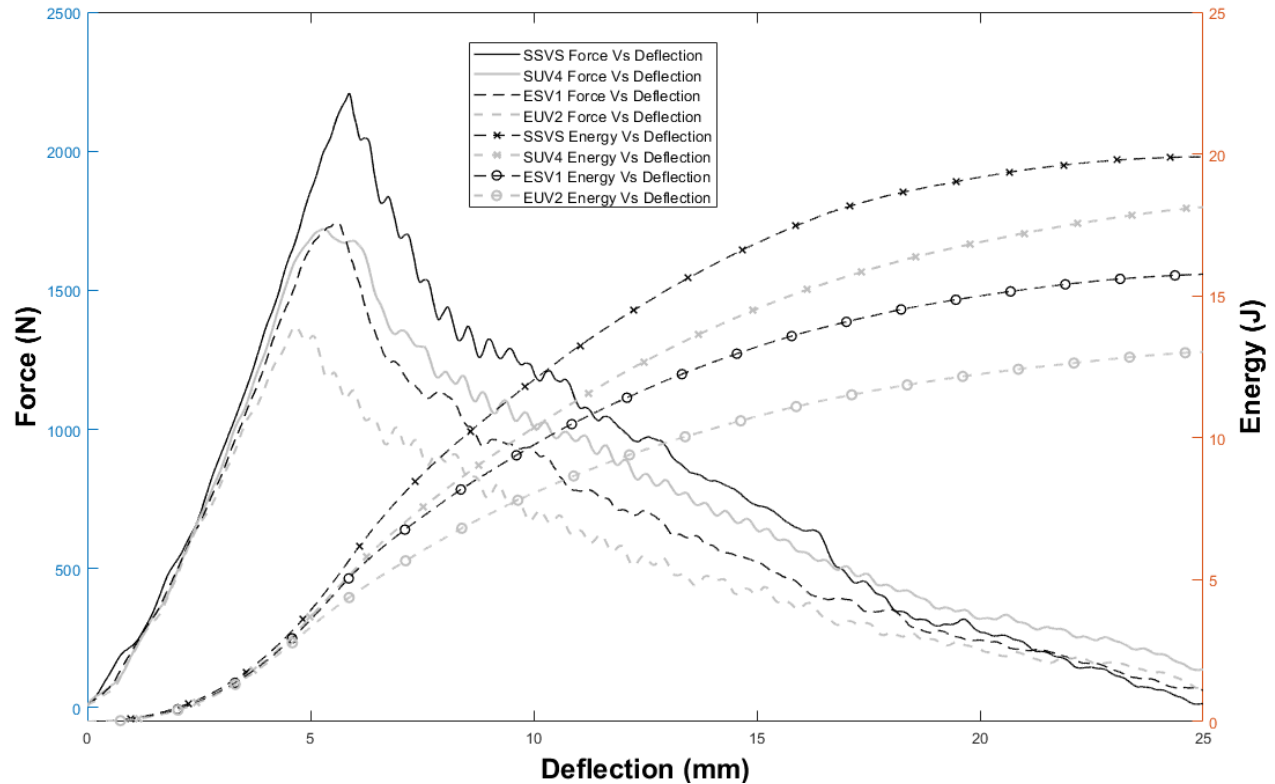
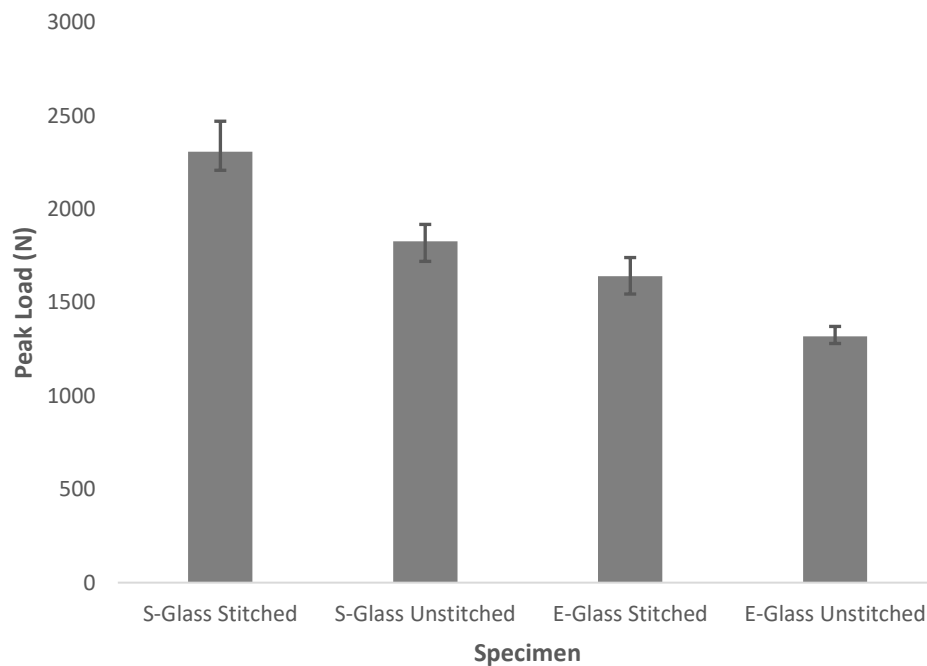


**Figure 18.** Comparison of Force, Energy and Deflection plots among representative specimens of E- and S- Glass/Vinyl Ester samples from low velocity punch- shear tests.

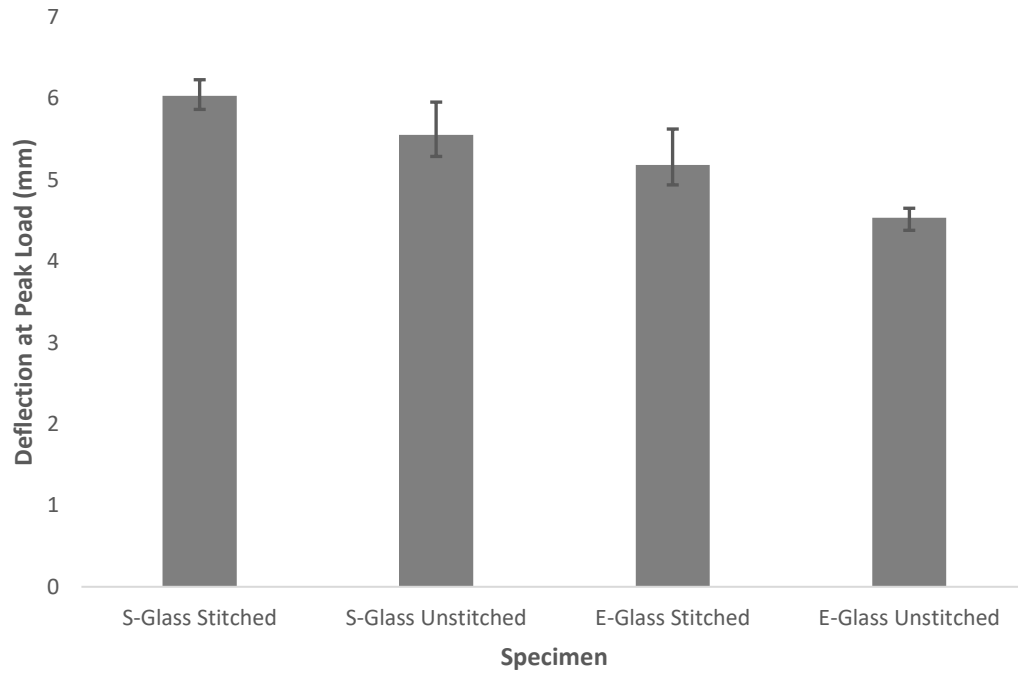
The peak load varies following the order:  $SSV > SUV > ESV > EUV$ . In some cases, the stitching is observed to play an even more dominant role where stitched E-Glass/Vinyl Ester specimens exhibit the same amount of energy absorption or peak force as the un-stitched S-Glass/Vinyl Ester specimens. Another key observation is the slightly steeper slope of the S-Glass/Vinyl Ester specimens compared to E-Glass/Vinyl Ester. This denotes higher stiffness for the former which is also in agreement with the vibration analysis results. However, the slope remains almost the same when comparing stitched and unstitched variants within the E- and S-Glass/Vinyl Ester specimens, only the peak force is higher for the stitched ones.

The force-deflection curves for all specimens appear symmetric up to a certain point with the absence of any stepped incipient damage initiation, which usually indicates an onset of matrix microcracking, fiber damage or delamination. This indicates complete puncture with little to no delamination and mostly brittle failure with the likelihood of delamination or fiber breakage occurring afterwards during puncture propagation.

**Figures 19 (a) and 19 (b)** illustrates the comparison of peak load and deflection at peak load of all the specimens with data scatter. **Figures 20(a) through 10(c)** depict the comparison of specific energy absorption i.e., energy absorption per unit mass during damage initiation and puncture propagation phases in order to better visualize the normalized energy absorption.

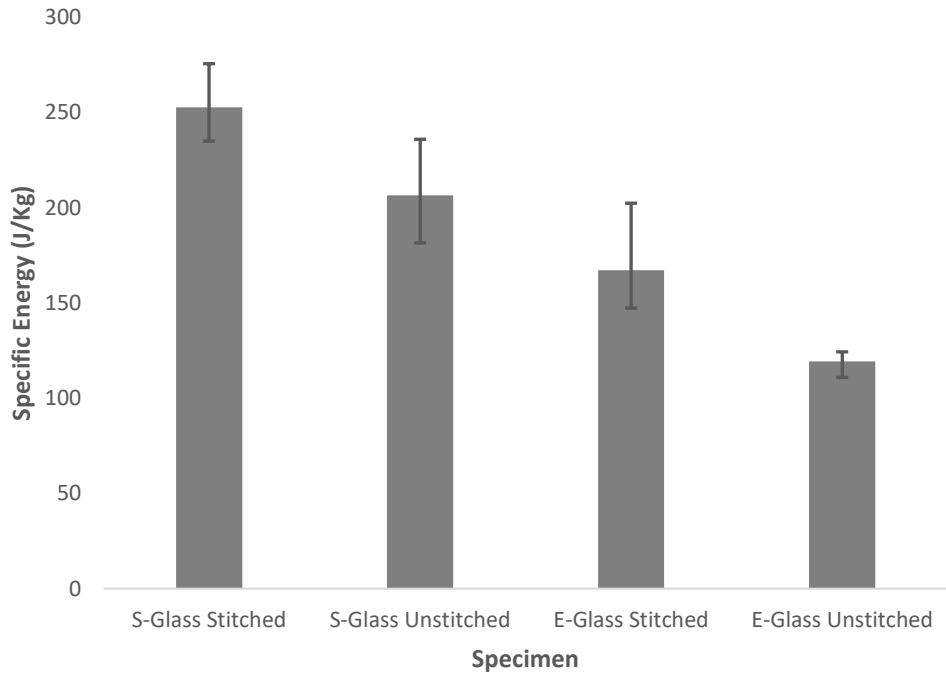


(a)

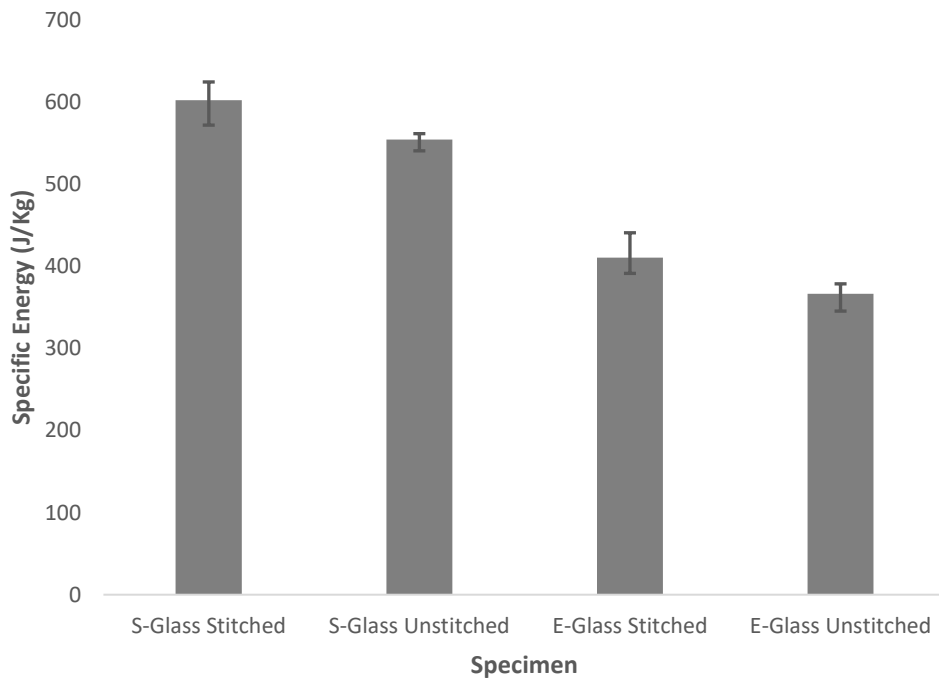


(b)

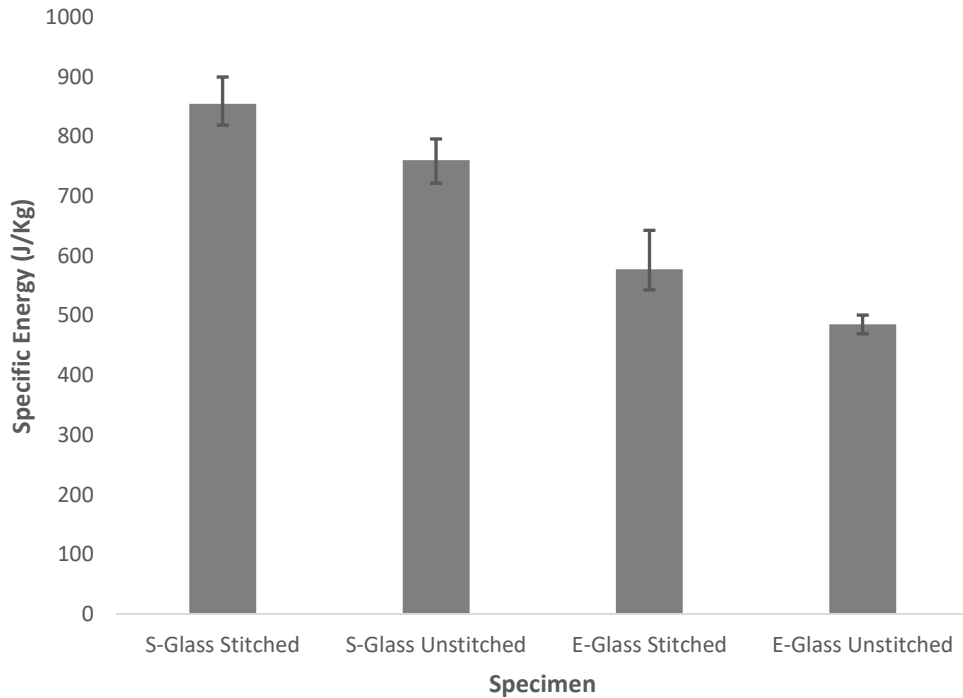
**Figure 19.** Comparison of (a) Peak load and (b) Deflection at peak load of the glass fiber reinforced specimens from low velocity punch-shear tests.



(a)



(b)



(c)

**Figure 20.** Comparison of (a) Specific energy at damage initiation, (b) Specific energy at puncture propagation, and (c) Total specific energy absorption of E- and S-Glass/Vinyl Ester specimens from low velocity punch-shear tests.

As seen from the figures, the specific energy absorption also follows the order  $SSV > SUV > ESV > EUV$ . There is an average of 18.4% increase in total energy absorption with stitching for E-Glass/Vinyl Ester specimens while an average of 12.4% increase is seen in the case of S-Glass/Vinyl Ester specimens. This goes to signify the contribution of stitching in through-thickness reinforcement for laminated GFRPs. For FRPS, major mechanisms of energy absorption are shear, delamination and elastic flexure [59]. Penetration may be influenced by fiber sizing, fiber orientation, type of weave, fiber-matrix interface etc. A fracture energy

calculation is also carried out based on a model of penetration provided by Dorey [57], in which the absorbed energy due to low-velocity impact is given by:

$$E = \pi \gamma t d \quad (13)$$

Where,  $\gamma$  = fracture energy,  $d$  = diameter of impactor, and  $t$  = plate thickness. The fracture energy calculation follows the same trend as the specific energy across all specimens. Compared to the unstitched E-Glass/Vinyl Ester specimens the stitched E-Glass/Vinyl Ester, unstitched and stitched S-Glass/Vinyl Ester specimens showed 41.4%, 79.3% and 112.6% increase in fracture energy respectively. This is shown in **Figure 21**.

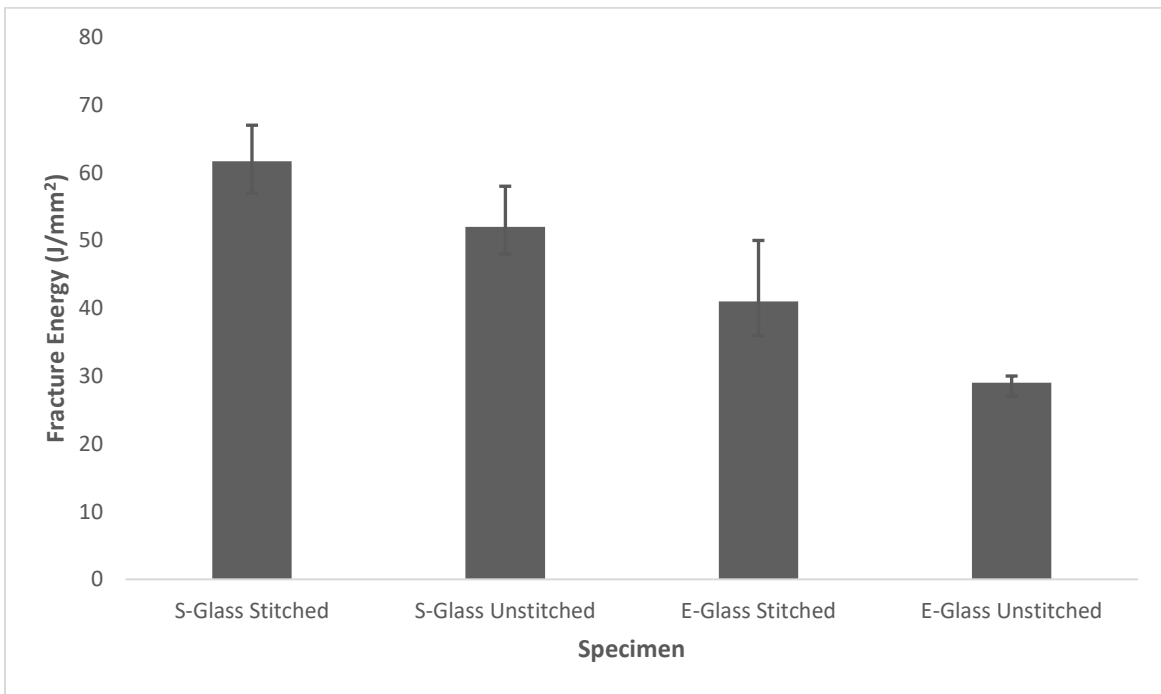
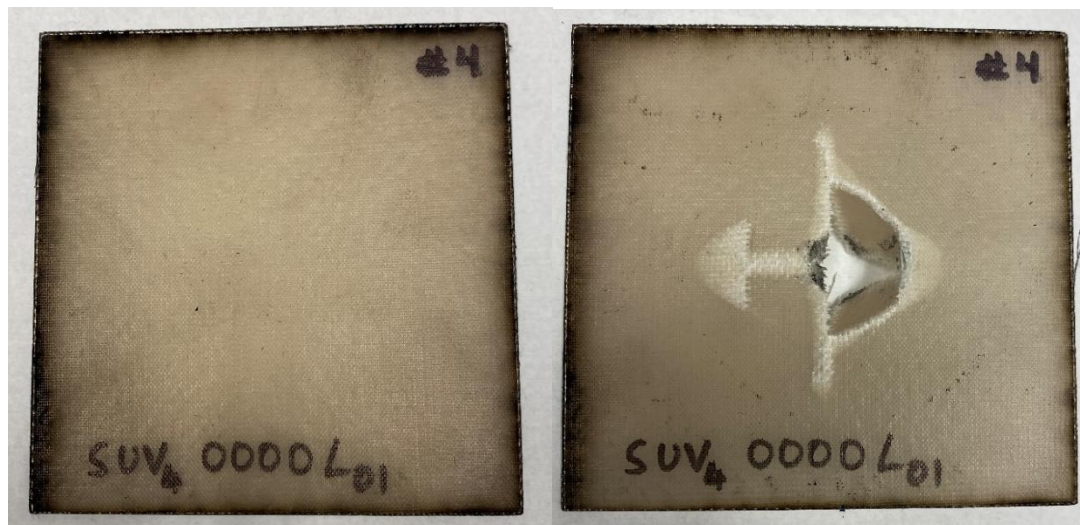


**Figure 21.** Comparison of Calculated Computed Fracture Energy of E- and S-Glass Vinyl Ester Specimens from low velocity punch-shear tests.

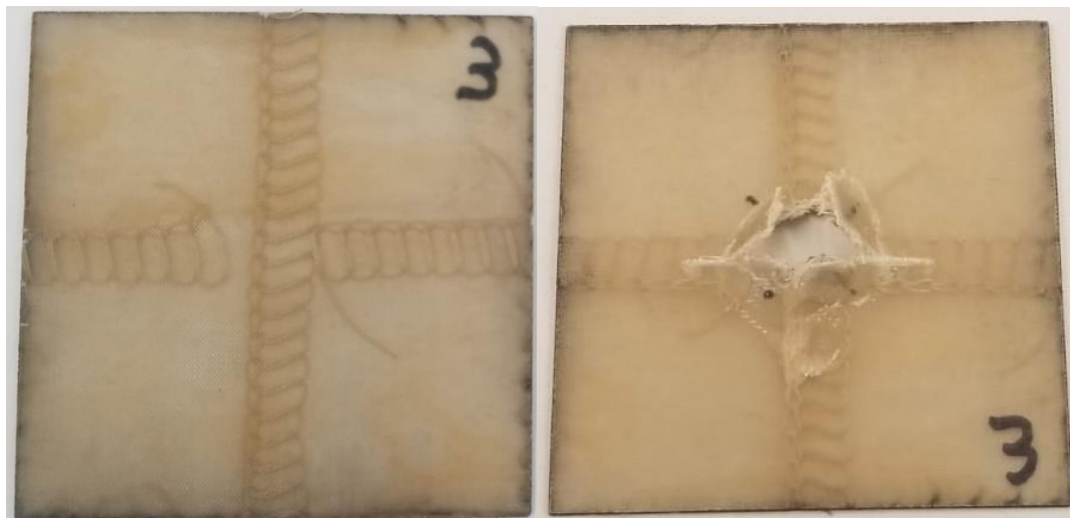
Post-test examination of the specimens reveal shear failure in the thickness direction with fibers breaking off from the weave creating a hexagonal zone at the back surface of each specimen with diametric cracks. **Figures 22(a-d)** show typical specimens after punch-shear experimentation.



(a)



(b)



(c)

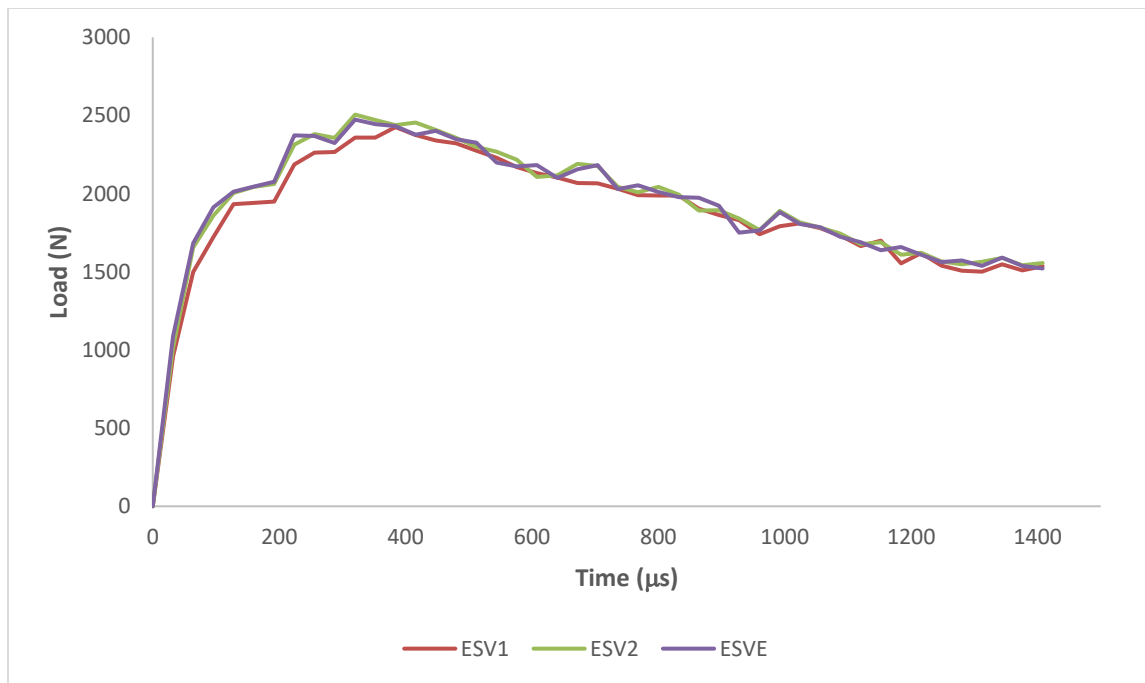


(d)

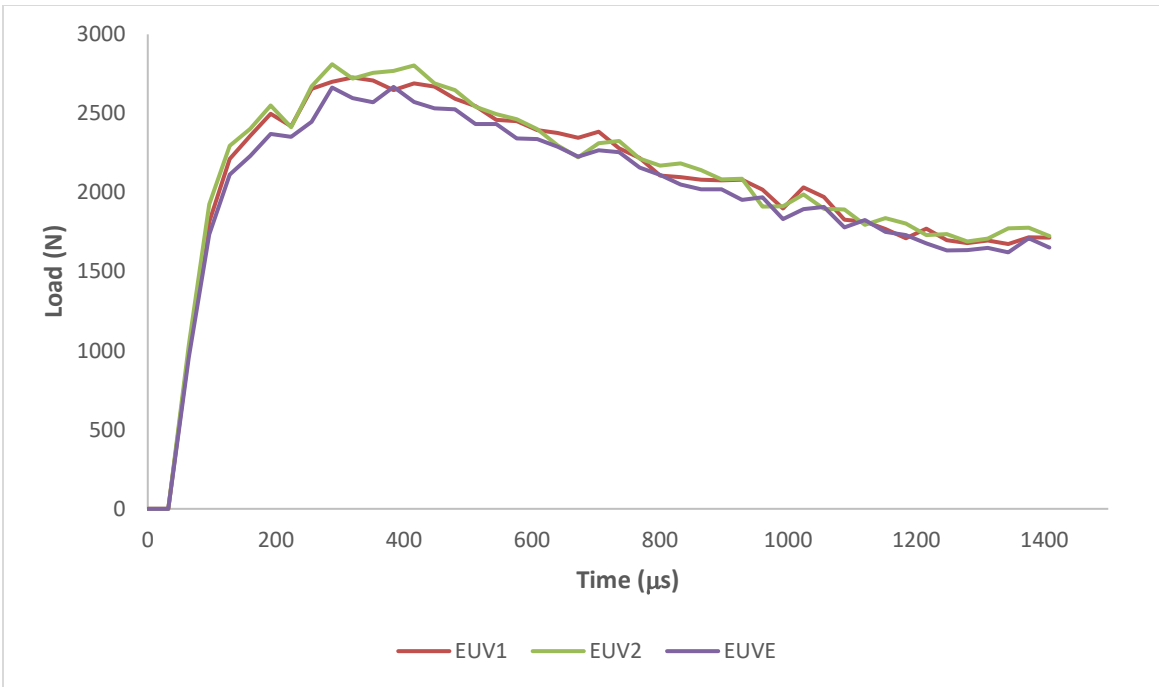
**Figure 22.** Low-velocity punch-shear test specimens before and after impact: (a) Stitched S-Glass/Vinyl Ester, (b) Unstitched S-Glass/Vinyl Ester, (c) Stitched E-Glass/Vinyl Ester, and (d) Un-stitched E-Glass/Vinyl Ester.

### 4.3 Shock Tube Data Analysis

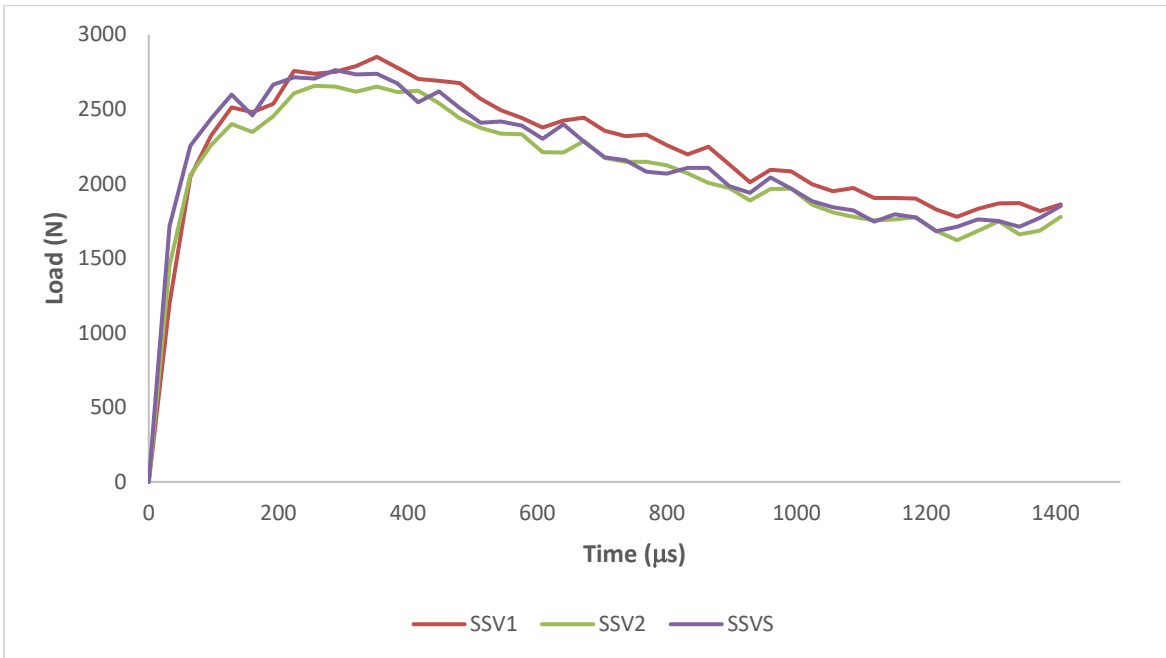
Shock loading of specimens was carried out in plate configuration with fixed circular boundary conditions. Transducers placed at appropriate locations along shock wave travel recorded the incident and reflected pulses while digital image captured by high-speed cameras set at an angle were used to calculate out of plane center point de-flection using 3D DIC software. Since the transducers and the recording devices operate at different sampling rates, a frame-to-frame comparison is done afterwards to synchronize the obtained data. Figures 23(a-e) show the load-time plots obtained from shock experiments. Based on the repeatability of the setup used for shock tests, there were minimal variations in the pressure profiles.



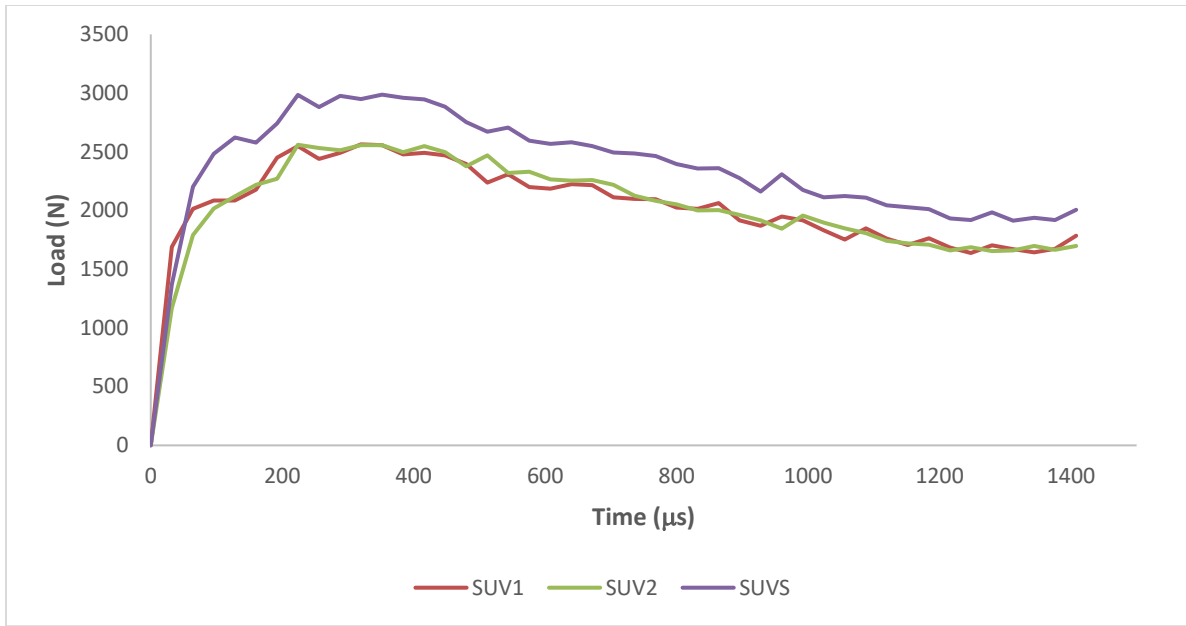
(a)



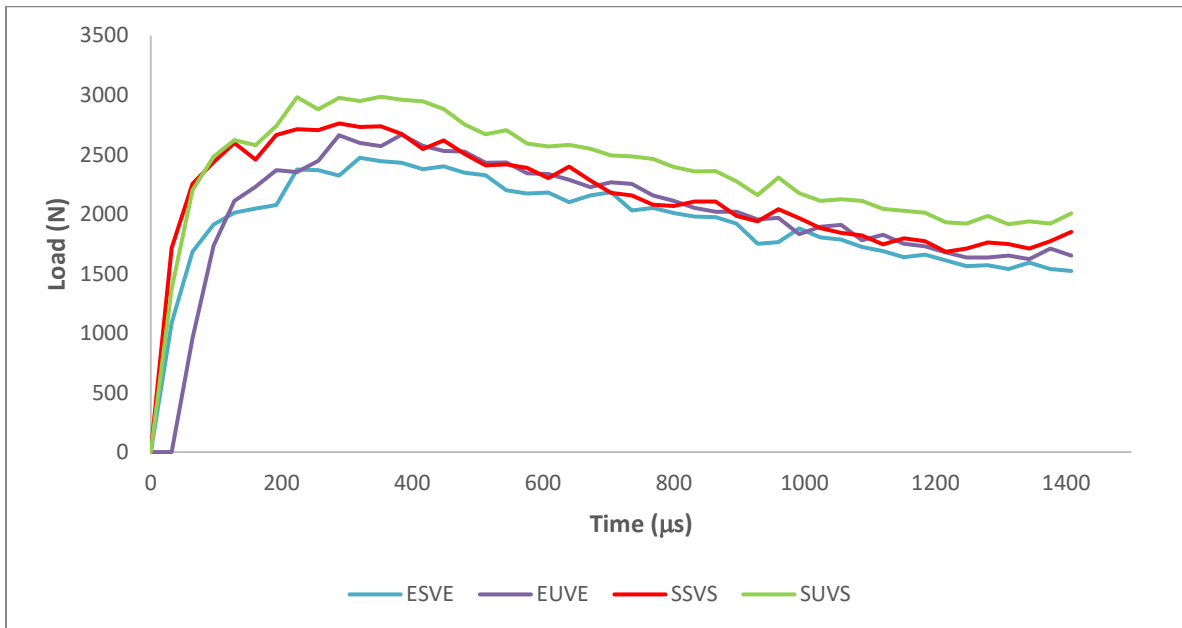
(b)



€



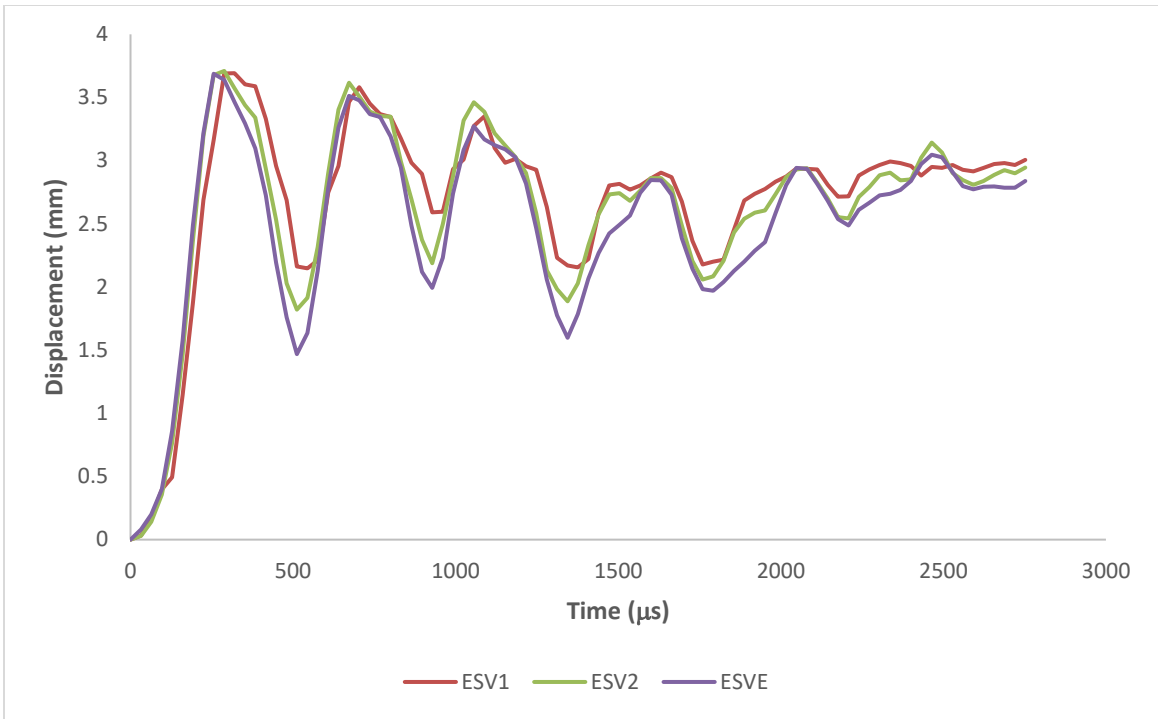
(d)



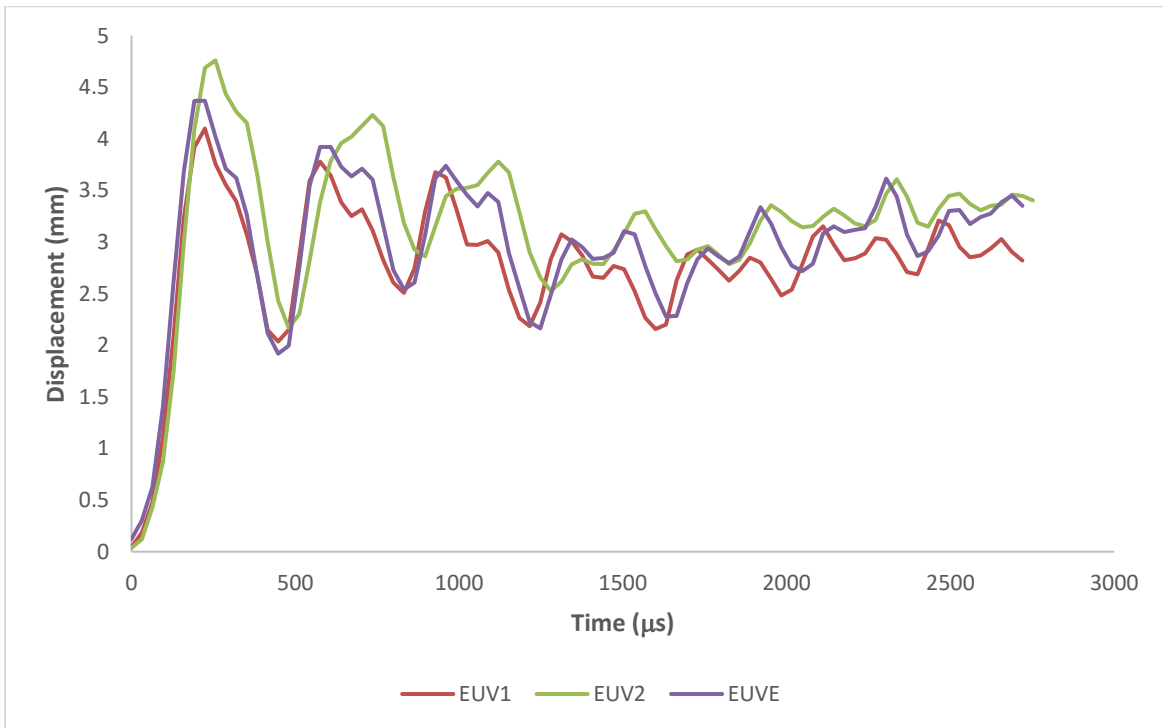
€

**Figure 23.** Load-Time response of (a) Stitched E-Glass/Vinyl Ester, (b) Unstitched E-Glass/Vinyl Ester, (c) Stitched S-Glass/Vinyl Ester and (d) Unstitched S-Glass/Vinyl Ester € All specimens averaged under shock loading.

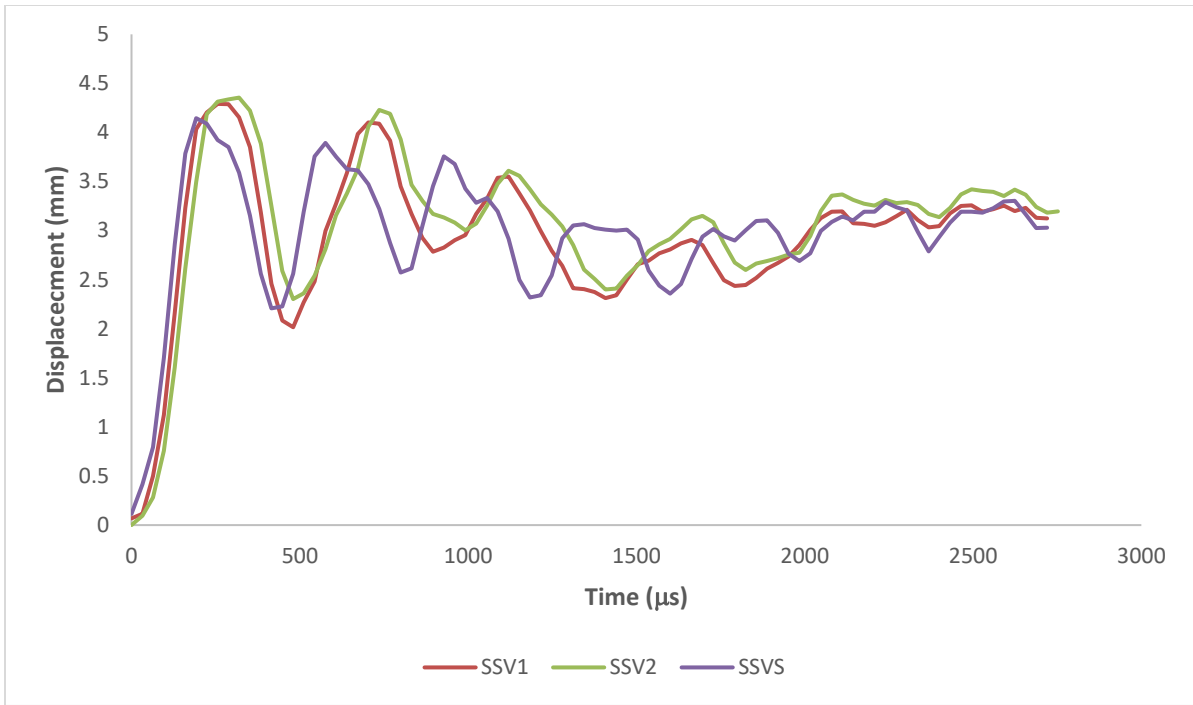
The primary objective was the center point deflection of the circular specimens under shock loading. The 3D DIC tool, GOM Correlate uses frame-by-frame data from 2 cameras and synchronizes them to create a 3D field of motion. It then tracks speckle patterns (put on the specimen using spray paint) along the Z-axis indicated normal to the specimen surface. The resolution of DIC tracking is based on the calibration done prior to testing using a calibration artifact provided by the software company. In this study, 4.2 MPa initial pressure was applied for shock loading the specimens which was not enough to cause failure. Rather, the specimens underwent oscillatory deformation and the geometric center point of the back surface of the specimen was used as reference to find the center point deflection. Trial points are placed around the geometric center in the DIC tool to locate the point of highest deformation, which essentially gives the center point deflection. Using the tool, the plots for deflection-time and load-deflection are obtained directly. **Figures 24(a-d)** show the deflection-time plots while and **Figure 25(e)** shows a comparative displacement-time plot among representative specimens of each type of composite sample.



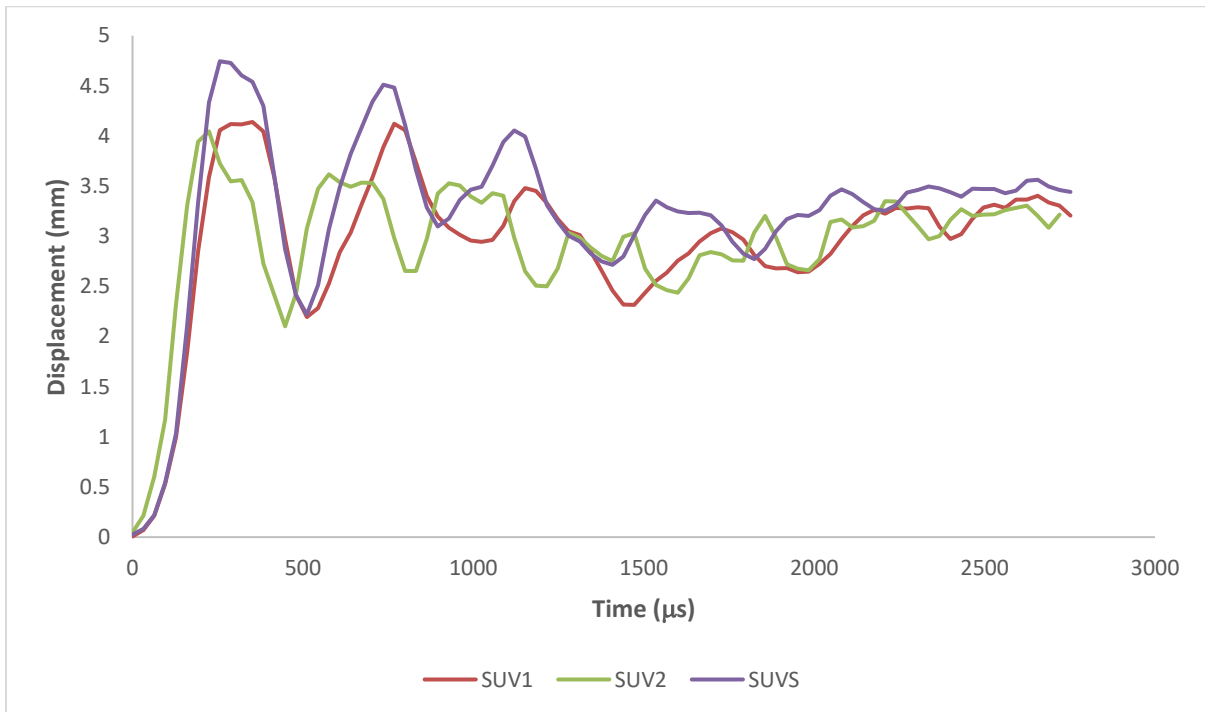
(a)



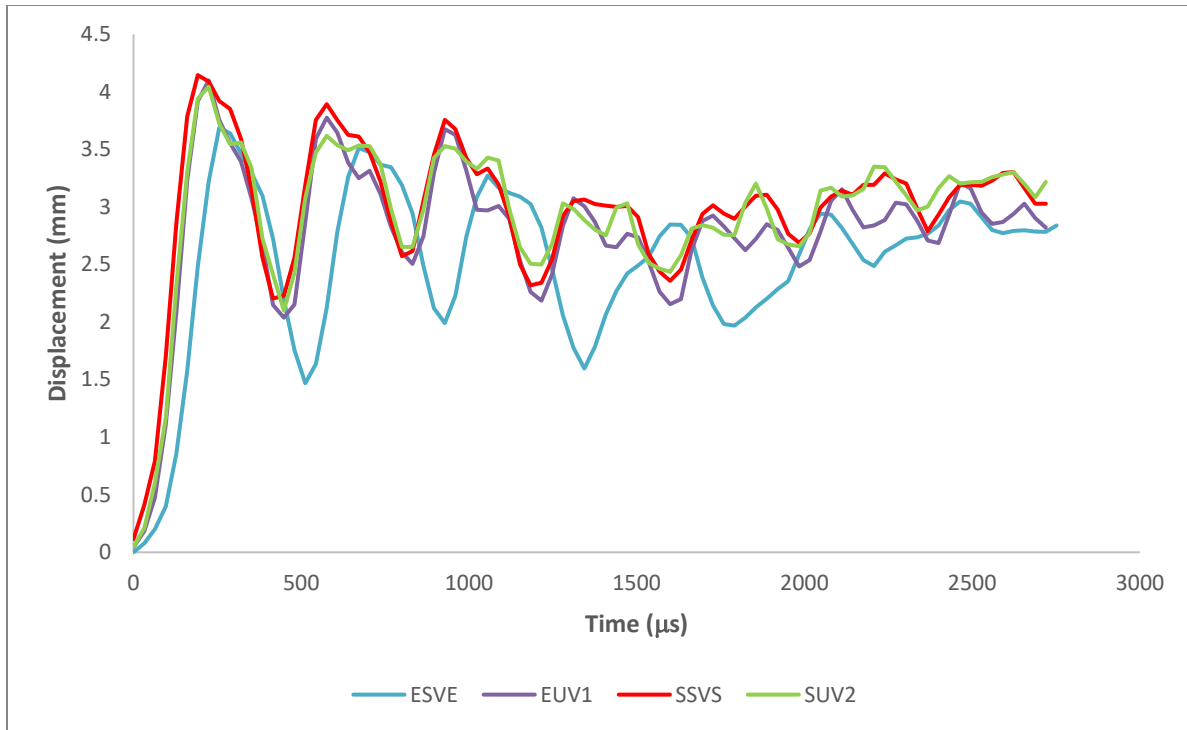
(b)



(c)



(d)

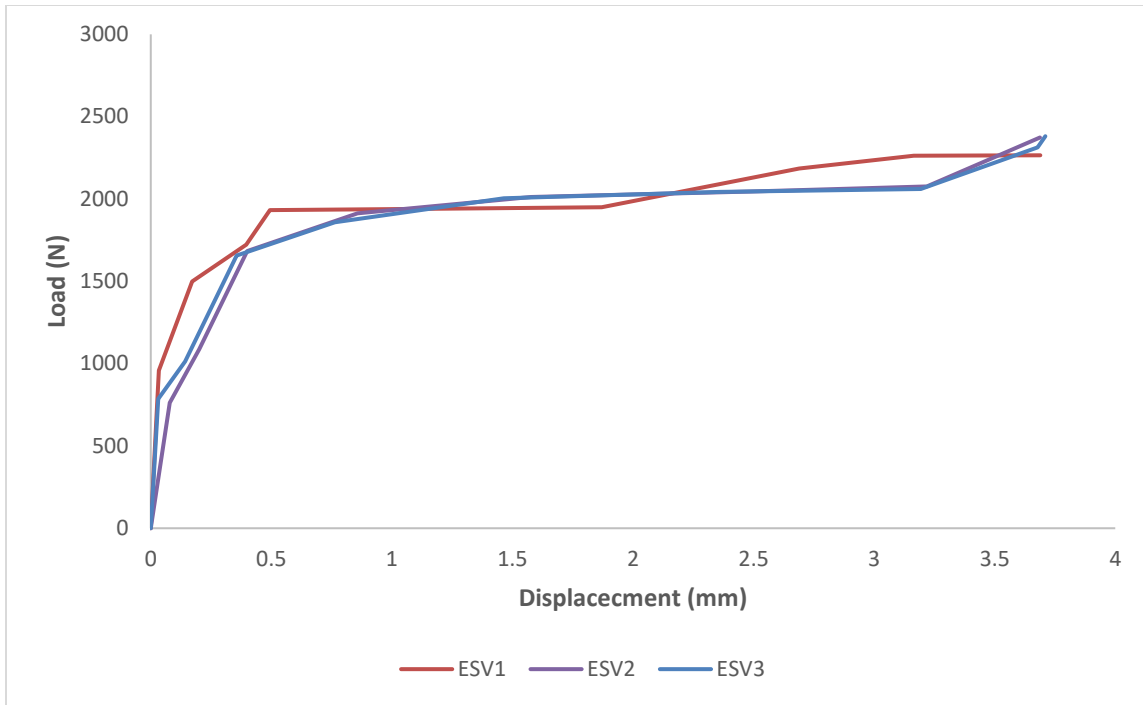


(e)

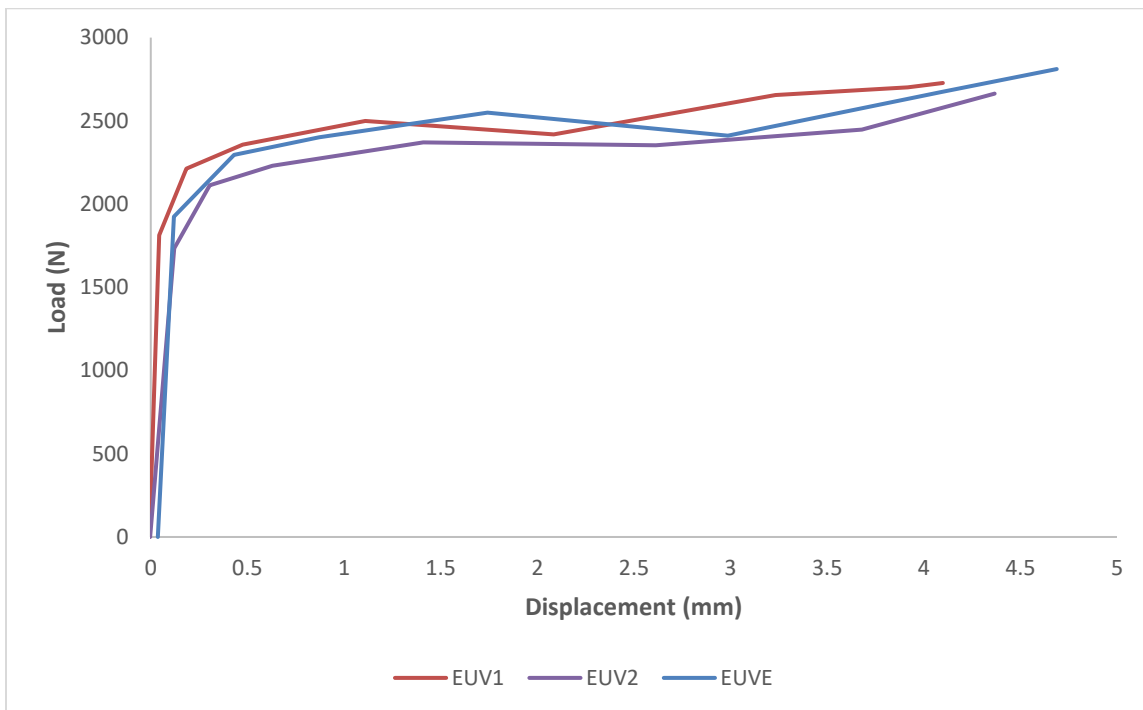
**Figure 24.** Displacement-Time response of (a) Stitched E-Glass/Vinyl Ester, (b) Unstitched E-Glass/Vinyl Ester, (c) Stitched S-Glass/Vinyl Ester and (d) Unstitched S-Glass/Vinyl Ester (e)

All specimens averaged under shock loading.

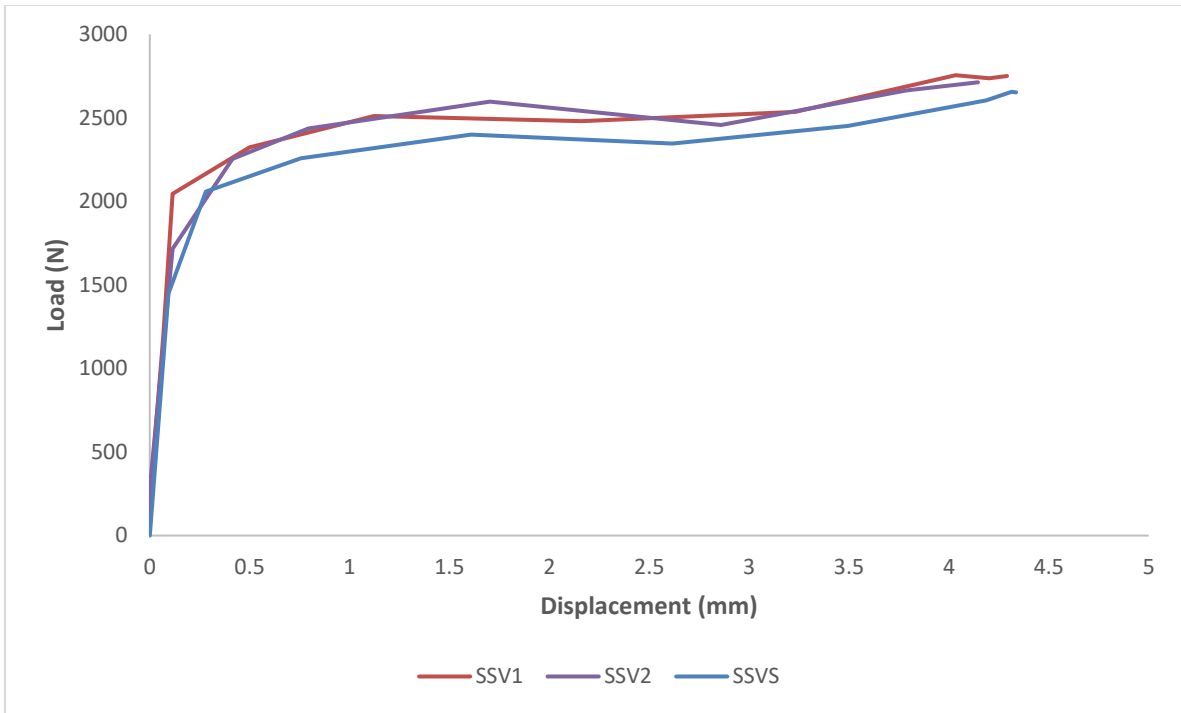
**Figures 25(a-d)** show the load-deflection curves along with a comparative load-deflection shown in **Figure 25(e)**.



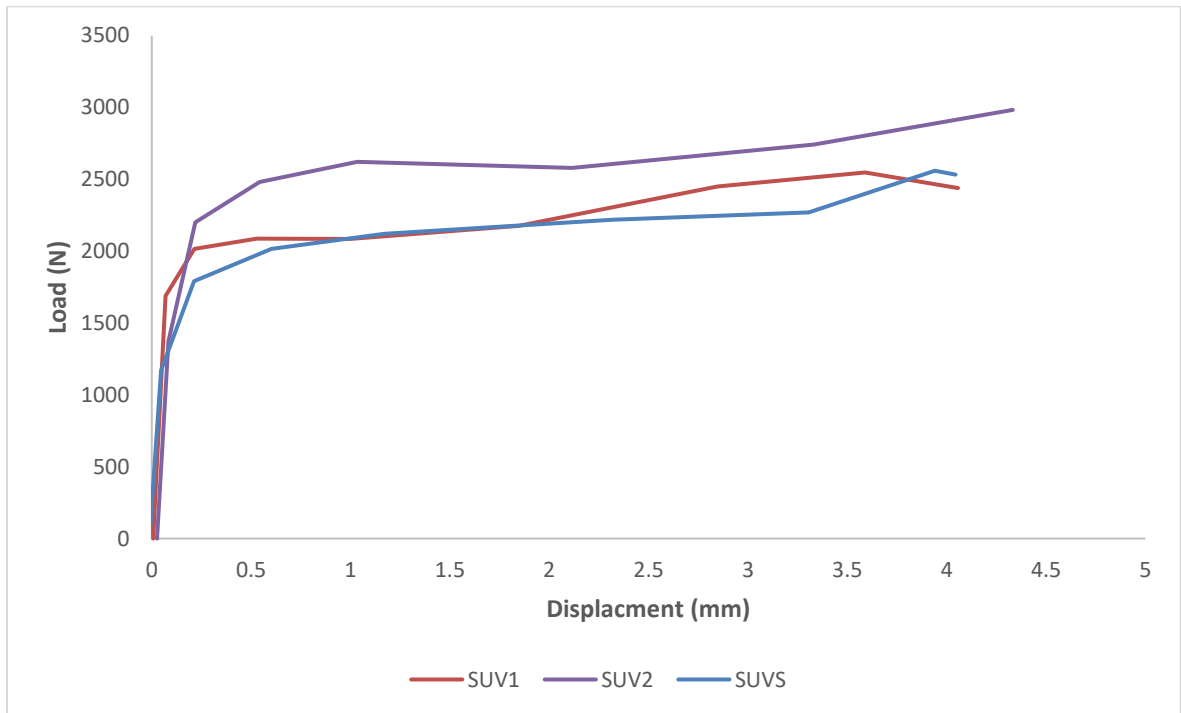
(a)



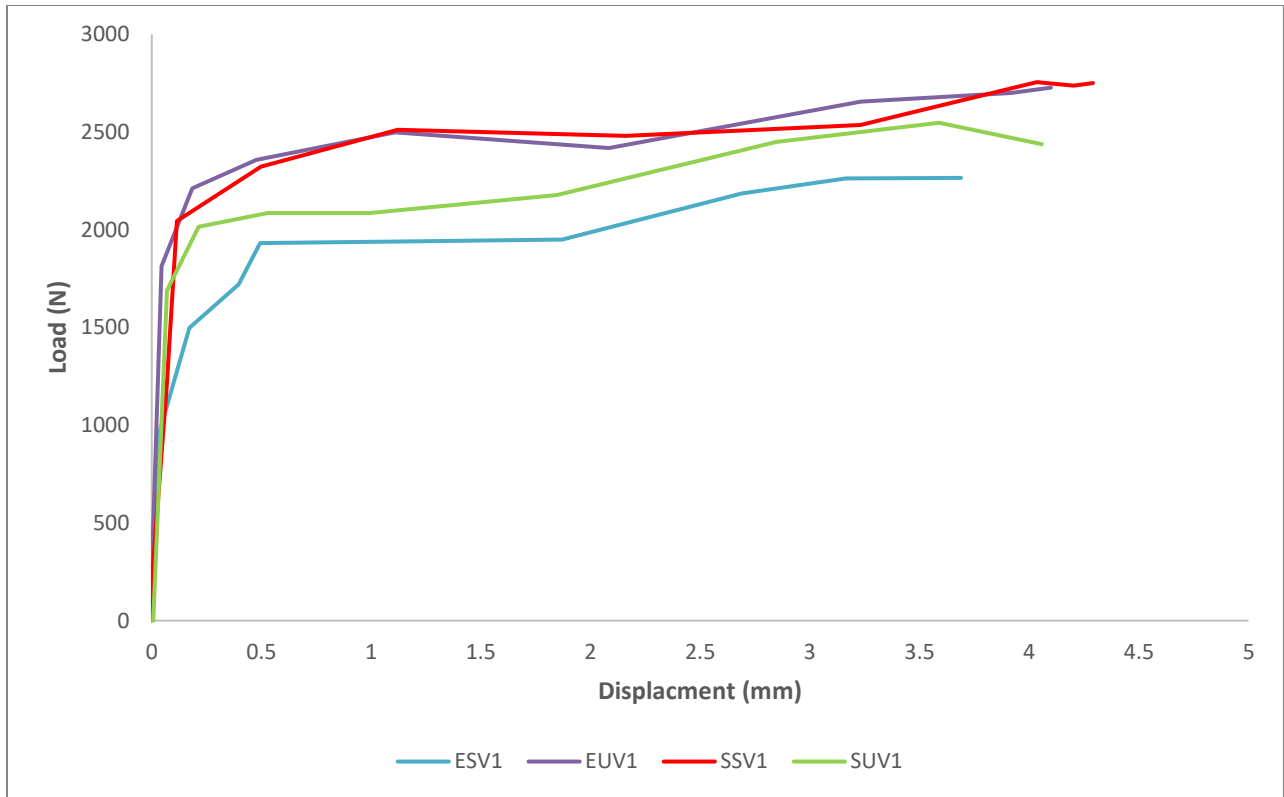
(b)



(c)



(d)



(e)

**Figure 25.** Load-Deflection response of (a) Unstitched S-Glass/Vinyl Ester, (b) Stitched S-Glass/Vinyl Ester, (c) Unstitched E-Glass/Vinyl Ester and (d) Stitched E-Glass/Vinyl Ester, and (e) All specimens averaged under shock loading.

From **Figure 25(e)**, it is observed that all the variants of composites have deflections between 4 and 4.5 mm except for the Stitched E-Glass/Vinyl Ester specimens which showed consistent deflections below 4 mm. The average deflections for all types of specimens are given in **Table 5**.

**Table 5.** Average Center Point Deflection of Different GFRP Specimens under shock loading.

Specimen Type	Average Center Point Deflection mm
Unstitched S-Glass/Vinyl Ester	4.31
Stitched S-Glass/Vinyl Ester	4.26
Unstitched E-Glass/Vinyl Ester	4.41
Stitched E-Glass/Vinyl Ester	3.69

As shown in **Table 5**, the center point deflections of stitched variants for both types of composites are less compared to their unstitched counterparts, indicating greater resistance to shock loading. The stitched E- Glass /Vinyl Ester samples had lowest deflection indicating highest resistance to shock loading. The average center point acceleration is given in **Figure 26**.

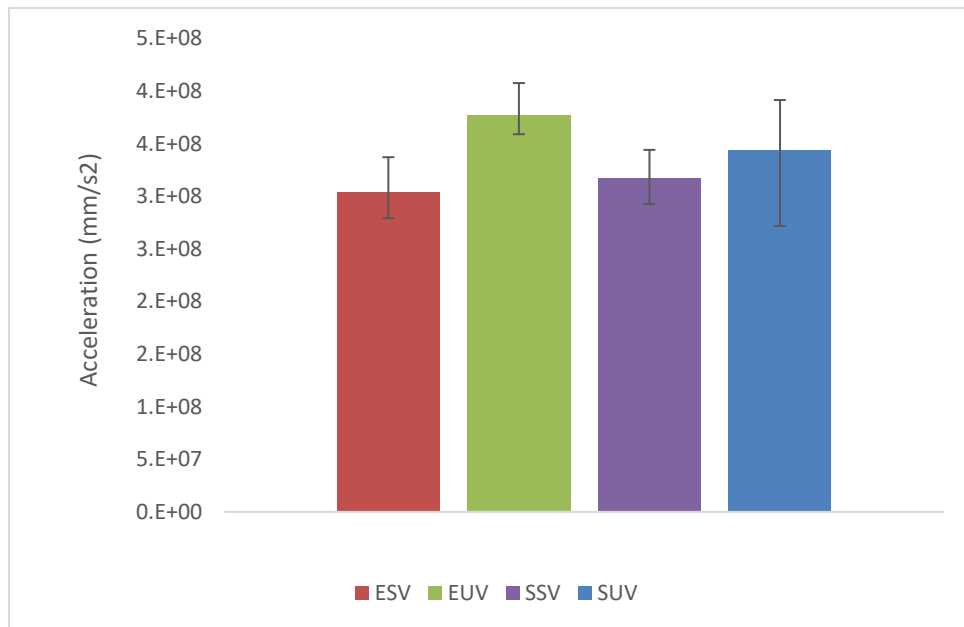


**Figure 26.** Average center point acceleration of the composite specimens under shock loading.

Average center point acceleration signifies the role stitching plays in the amount of deformation. The ones without stitching exhibit greater accelerations revealing the effectiveness of through the ply stitching in resisting shock load. Also, the stiffer S-Glass/Vinyl Ester composites exhibited less acceleration under shock loading. The average energy absorption up to the point of maximum deflection was calculated and shown in **Figure 17**. This follows the same trend as average deflection data, with the stitched E-Glass/Vinyl Ester specimens absorbing the least amount of energy.

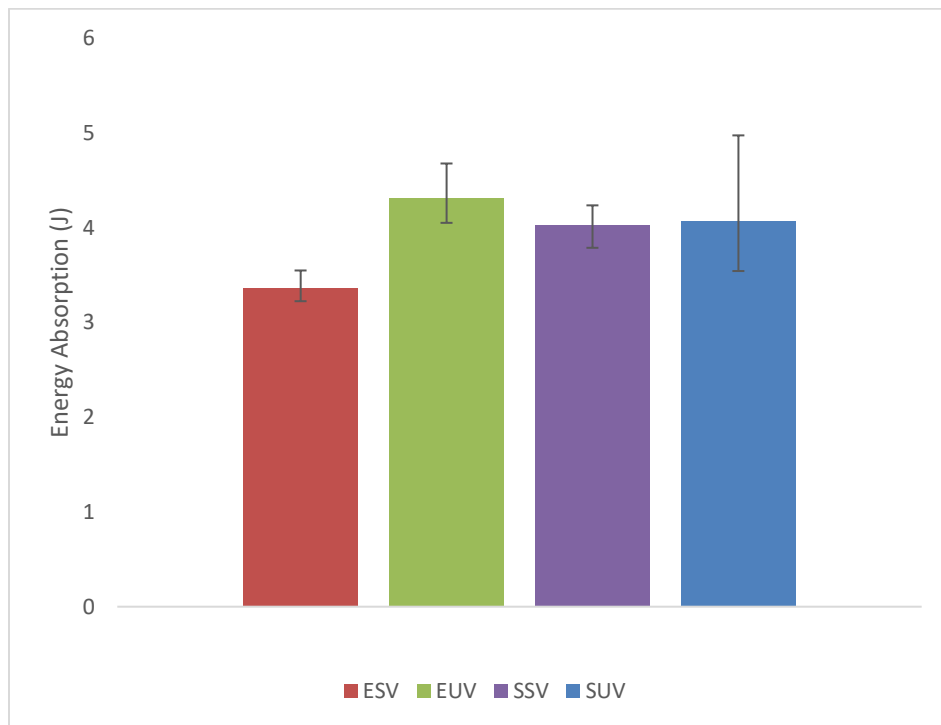


**Figure 27.** Average energy absorption up to point of maximum deflection of composite specimens under shock loading.

Based on the collective evaluation of the shock loading data, an apparent conjecture can be made: while the stitching helps increase through thickness reinforcement and resist the effects of delamination or fiber breakage, it may also introduce regions of stress concentration in the matrix which could potentially lead to lower overall strength and premature failure. But this may also be influenced by the quality of stitching and the interface between the stitch material and the matrix resin.

CHAPTER V  
CONCLUSION

**5.1 Vibration Analysis**

- Results from vibration analysis of stitched specimens show increase in natural frequency and dynamic flexural modulus for the stitched specimens compared to the un-stitched ones for both E- and S-Glass/Vinyl Ester composites.
- The resonant frequencies were found to be approximately 31 Hz for unstitched and 34 Hz for stitched E-Glass/Vinyl Ester while approximately 34 Hz for unstitched and 37 Hz for stitched S-Glass/Vinyl Ester specimens
- While there were noticeable changes in dynamic moduli; loss factors (damping) showed little to no change.

**5.2 Low-Velocity Impact**

- Low-velocity punch shear testing showed that stitching improved energy absorption along the thickness direction.
- Approximately 20% increase in total energy absorption was noticed for E-Glass/Vinyl Ester and 12 % for S-Glass/Vinyl Ester due to stitching.
- With unstitched E-Glass/Vinyl Ester specimens as the baseline; the stitched E-Glass/Vinyl Ester, unstitched, and stitched S-Glass/Vinyl Ester specimens showed 40%,

80% and 115% increase in fracture energy respectively.

- The stitched S- Glass/Vinyl Ester therefore showing an increase of approximately 30% fracture energy from the unstitched ones.

### **5.3 Shock Analysis**

- Shock loading of the circular FRP plates was unable to achieve damage and fail the specimens. Rather, there was a vibratory deflection that was recorded and calculated using 3D DIC tool.
- While the load-deflection curves followed almost similar trends, the average center point deflection appeared to be lower for stitched specimens compared to their unstitched counterparts.
- The average center point deflection for unstitched E-Glass/Vinyl Ester as well as stitched and unstitched S-Glass/Vinyl Ester ranged from 4 mm to 4.5 mm; with the stitched E-Glass/Vinyl Ester deflecting lower to about 3.7 mm, demonstrating higher resistance to shock loading.
- On the other hand, unstitched specimens absorbed more energy up to maximum deflection point than the stitched variants with the stitched E-Glass/Vinyl Ester having lowest energy absorption.

#### **5.4 Recommendation for Future Research**

Based on results obtained from this relatively small sample size, it is hard to draw definitive conclusions as to how much of an impact through thickness stitching has on strengthening the composite properties under shock loading scenario. Further comparative investigations into the properties of E- and S-Glass/Vinyl Ester would be recommended with an adequate sample size to account for all probable variations and outliers.

It is also recommended to carry out material characterization tests such as high strain rate tensile/compression (e.g., on a Split Hopkinson Pressure Bar apparatus), direct impact tests as opposed to the tests for particular configuration carried out in this study. In addition, computational analysis is highly significant to validate and simulate similar scenarios with controllable parameters. Apart from testing separately, it is also worth investigating the different load responses of these GFRPs as skins of sandwich structures such as that seen in many foam core sandwich composites with variable number of layers.

## REFERENCES

1. Ravindran, Naveenkamal, "Durability of E-glass fiber reinforced vinyl ester polymer composites with nanoclay in an alkaline environment" (2005). Graduate Theses, Dissertations, and Problem Reports. 1640. <https://researchrepository.wvu.edu/etd/1640>
2. B. Stankiewicz, Composite GFRP Deck for Bridge Structures, *Procedia Engineering*, Volume 40, 2012, Pages 423-427, ISSN 1877-7058, <https://doi.org/10.1016/j.proeng.2012.07.119>.
3. Quilter, Adam. "Composites in Aerospace Applications" *AviationPros*, 1 October, 2004, <https://www.aviationpros.com/engines-components/aircraft-airframe-accessories/article/10386441/composites-in-aerospace-applications>
4. Ghobadi, A. (2017) Common Type of Damages in Composites and Their Inspections. *World Journal of Mechanics*, 7, 24-33. doi: 10.4236/wjm.2017.72003. <https://doi.org/10.4236/wjm.2017.72003>
5. Arbaoui, J., Tarfaoui, M., Bouery, C., & El Malki Alaoui, A. (2016). Comparative study of mechanical properties and damage kinetics of two and three-dimensional woven composites under high-strain rate dynamic compressive loading. *International Journal of Damage Mechanics*, 25(6), 878-899. <https://doi.org/10.1177/1056789516651691>
6. Mouritz, A. P., Leong, K. H., & Herszberg, I. (1997). A review of the effect of stitching on the in-plane mechanical properties of fiber-reinforced polymer composites. *Composites Part A: applied science and manufacturing*, 28(12), 979-991. [https://doi.org/10.1016/S1359-835X\(97\)00057-2](https://doi.org/10.1016/S1359-835X(97)00057-2)

7. Mouritz, A. P. (2001). Ballistic impact and explosive blast resistance of stitched composites. *Composites Part B: Engineering*, 32(5), 431-439.  
[https://doi.org/10.1016/S1359-8368\(01\)00015-4](https://doi.org/10.1016/S1359-8368(01)00015-4)
8. Gibson, R. F., & Plunkett, R. (1976). Dynamic mechanical behavior of fiber-reinforced composites: measurement and analysis. *Journal of Composite Materials*, 10(4), 325-341.  
<https://doi.org/10.1177/002199837601000406>
9. Gibson, R. F. (1992). Dynamic mechanical behavior of composite materials and structures (No. 921094). SAE Technical Paper. <https://doi.org/10.4271/921094>
10. Gibson, R.F. 'Principles of Composite Material Mechanics' McGraw-Hill, 1992
11. Hwang, S. J., & Gibson, R. F. (1993). Prediction of fiber-matrix interphase effects on damping of composites using a micromechanical strain energy/finite element approach. *Composites Engineering*, 3(10), 975-984. [https://doi.org/10.1016/0961-9526\(93\)90005-5](https://doi.org/10.1016/0961-9526(93)90005-5)
12. Suarez, S. A., Gibson, R. F., & Deobald, L. R. (1984). Random and impulse techniques for measurement of damping in composite materials. *Experimental Techniques*, 8(10), 19-24. <https://doi.org/10.1111/j.1747-1567.1984.tb01832.x>
13. Barpanda, D., & Mantena, P. R. (1996). Dynamic mechanical analysis of pultruded glass-graphite/epoxy hybrid composites at elevated temperatures. *Journal of reinforced plastics and composites*, 15(5), 497-532. <https://doi.org/10.1177/073168449601500504>
14. Al-Ostaz, A., Mantena, P. R., Anakapalli, M., & Hwang, S. J. (2007). Evaluation of high-performance pressure-sensitive adhesives and VHB™ acrylic foam tapes bonded aluminum joints subjected to environmental aging. *Journal of adhesion science and technology*, 21(3-4), 339-361. <https://doi.org/10.1163/156856107780684576>

15. Nori, C. V., Mantena, P. R., & McCarty, T. A. (1996). Experimental and finite element analysis of pultruded glass-graphite/epoxy hybrids in axial and flexural modes of vibration. *Journal of composite materials*, 30(18), 1996-2018.  
<https://doi.org/10.1177/002199839603001803>
16. Mantena, P. R., Al-Ostaz, A., & Cheng, A. H. (2009). Dynamic response and simulations of nanoparticle-enhanced composites. *Composites science and technology*, 69(6), 772-779. <https://doi.org/10.1016/j.compscitech.2008.02.035>
17. Mantena, P.R., Gibson, R.F. Place, T. and Alan. A torsional impulse-frequency response technique for evaluating the dynamic mechanical properties of structural materials, In'Proc, of the 6th Annual ASM/ESD Advanced Comp. Conf ", Detroit, MI, 1990, pp. 477 485
18. Kumar, S., & Mantena, P. (1994). Characterization of dynamic mechanical properties of pultruded hybrid cylindrical composite rods in the torsional mode of vibration. In 35th Structures, Structural Dynamics, and Materials Conference (p. 1461).  
<https://doi.org/10.2514/6.1994-1461>
19. Mantena, P. R., Mann, R., & Nori, C. (2001). Low-velocity impact response and dynamic characteristics of glass-resin composites. *Journal of reinforced plastics and composites*, 20(6), 513-534. <https://doi.org/10.1177/073168401772678689>
20. Li, N., Tahar, M. B., Aboura, Z., & Khellil, K. (2016). A dynamic analysis approach for identifying the elastic properties of unstitched and stitched composite plates. *Composite Structures*, 152, 959-968. <https://doi.org/10.1016/j.compstruct.2016.06.038>
21. Wu, J., & Moslehy, F. A. (1995). On modal testing using speaker for excitation. In *Proceedings of the 13th International Modal Analysis Conference (Vol. 2460, p. 24)*.

22. Araujo, A. L., Soares, C. M., de Freitas, M. M., Pedersen, P., & Herskovits, J. (2000). Combined numerical experimental model for the identification of mechanical properties of laminated structures. *Composite Structures*, 50(4), 363-372. [https://doi.org/10.1016/S0263-8223\(00\)00113-6](https://doi.org/10.1016/S0263-8223(00)00113-6)
23. De Baere, I., Van Paepegem, W., Degrieck, J., Sol, H., Van Hemelrijck, D., & Petreli, A. (2007). Comparison of different identification techniques for measurement of quasi-zero Poisson's ratio of fabric-reinforced laminates. *Composites Part A: Applied Science and Manufacturing*, 38(9), 2047-2054. <https://doi.org/10.1016/j.compositesa.2007.04.012>
24. Matter, M., Gmür, T., Cugnoni, J., & Schorderet, A. (2007). Improved modal characterization of the constitutive parameters in multilayered plates. *Composites science and technology*, 67(6), 1121-1131. <https://doi.org/10.1016/j.compscitech.2006.05.016>
25. Shi, Y., Sol, H., & Hua, H. (2005). Transverse shear modulus identification by an inverse method using measured flexural resonance frequencies from beams. *Journal of sound and vibration*, 285(1-2), 425-442. <https://doi.org/10.1016/j.jsv.2004.03.074>
26. Abrate, S. (1991). Impact on laminated composite materials. <https://doi.org/10.1115/1.3119500>
27. Abrate, S. (1994). Impact on laminated composites: recent advances. <https://doi.org/10.1115/1.3111065>
28. Abrate, S. (2001). Modeling of impacts on composite structures. *Composite structures*, 51(2), 129-138. [https://doi.org/10.1016/S0263-8223\(00\)00138-0](https://doi.org/10.1016/S0263-8223(00)00138-0)
29. Abrate, S. (1991). Matrix cracking in laminated composites: a review. *Composites engineering*, 1(6), 337-353. [https://doi.org/10.1016/0961-9526\(91\)90039-U](https://doi.org/10.1016/0961-9526(91)90039-U)

30. Schoeppner, G. A., & Abrate, S. (2000). Delamination threshold loads for low velocity impact on composite laminates. *Composites Part A: applied science and manufacturing*, 31(9), 903-915. [https://doi.org/10.1016/S1359-835X\(00\)00061-0](https://doi.org/10.1016/S1359-835X(00)00061-0)
31. Wyrick, D. A., & Adams, D. F. (1988). Damage sustained by a carbon/epoxy composite material subjected to repeated impact. *Composites*, 19(1), 19-27. [https://doi.org/10.1016/0010-4361\(88\)90540-X](https://doi.org/10.1016/0010-4361(88)90540-X)
32. Hosur, M. V., Vaidya, U. K., Ulven, C., & Jeelani, S. (2004). Performance of stitched/unstitched woven carbon/epoxy composites under high velocity impact loading. *Composite Structures*, 64(3-4), 455-466. <https://doi.org/10.1016/j.compstruct.2003.09.046>
33. Hosur, M. V., Karim, M. R., & Jeelani, S. (2003). Experimental investigations on the response of stitched/unstitched woven S2-glass/SC15 epoxy composites under single and repeated low velocity impact loading. *Composite structures*, 61(1-2), 89-102. [https://doi.org/10.1016/S0263-8223\(03\)00032-1](https://doi.org/10.1016/S0263-8223(03)00032-1)
34. Hosur, M. V., Adya, M., Alexander, J., Jeelani, S., Vaidya, U., & Mayer, A. (2003). Studies on impact damage resistance of affordable stitched woven carbon/epoxy composite laminates. *Journal of reinforced plastics and composites*, 22(10), 927-952. <https://doi.org/10.1177/0731684403022010005>
35. Hosur, M. V., Karim, M. R., & Jeelani, S. (2004). Studies on stitched woven S2 glass/epoxy laminates under low velocity and ballistic impact loading. *Journal of reinforced plastics and composites*, 23(12), 1313-1323. <https://doi.org/10.1177/0731684404037048>

36. Kang, T. J., & Lee, S. H. (1994). Effect of stitching on the mechanical and impact properties of woven laminate composite. *Journal of composite materials*, 28(16), 1574-1587. <https://doi.org/10.1177/002199839402801604>
37. PELSTRING, R., & MADAN, R. (1989). Stitching to improve damage tolerance of composites. In *International SAMPE Symposium and Exhibition, 34 th, Reno, NV* (pp. 1519-1528).
38. Glaessgen, E. H., Raju, I. S., & Poe Jr, C. C. (2002). Analytical and experimental studies of the debonding of stitched and unstitched composite joints. *Journal of Composite Materials*, 36(23), 2599-2622.
39. Liu, D. (1990). Delamination resistance in stitched and unstitched composite plates subjected to impact loading. *Journal of Reinforced Plastics and Composites*, 9(1), 59-69.
40. Dransfield, K., Baillie, C., & Mai, Y. W. (1994). Improving the delamination resistance of CFRP by stitching—a review. *Composites Science and Technology*, 50(3), 305-317.
41. Sha, G., Cao, M., Radziński, M., & Ostachowicz, W. (2019). Delamination-induced relative natural frequency change curve and its use for delamination localization in laminated composite beams. *Composite Structures*, 230, 111501.
42. Zou, Y., Tong, L. P. S. G., & Steven, G. P. (2000). Vibration-based model-dependent damage (delamination) identification and health monitoring for composite structures—a review. *Journal of Sound and vibration*, 230(2), 357-378.
43. Fan, W., & Qiao, P. (2011). Vibration-based damage identification methods: a review and comparative study. *Structural health monitoring*, 10(1), 83-111.
44. Pardoen, G. C. (1989). Effect of delamination on the natural frequencies of composite laminates. *Journal of composite materials*, 23(12), 1200-1215.

45. Kudela, P., Radzienski, M., & Ostachowicz, W. (2018). Impact induced damage assessment by means of Lamb wave image processing. *Mechanical Systems and Signal Processing*, 102, 23-36.
46. Yelve, N. P., Mitra, M., & Mujumdar, P. M. (2017). Detection of delamination in composite laminates using Lamb wave based nonlinear method. *Composite Structures*, 159, 257-266.
47. Angelidis, N., & Irving, P. E. (2007). Detection of impact damage in CFRP laminates by means of electrical potential techniques. *Composites Science and Technology*, 67(3-4), 594-604.
48. Glass, I. I., & Patterson, G. N. (1955). A theoretical and experimental study of shock-tube flows. *Journal of the Aeronautical Sciences*, 22(2), 73-100.  
<https://doi.org/10.2514/8.3282>
49. Aune, V., Fagerholt, E., Langseth, M., & Børvik, T. (2016). A shock tube facility to generate blast loading on structures. *International Journal of Protective Structures*, 7(3), 340-366. <https://doi.org/10.1177/2041419616666236>
50. Erheng Wang; Arun Shukla (2010). Analytical and experimental evaluation of energies during shock wave loading. , 37(12), 1188-1196. doi:10.1016/j.ijimpeng.2010.07.003  
<https://doi.org/10.1016/j.ijimpeng.2010.07.003>
51. Tekalur, S. A., Bogdanovich, A. E., & Shukla, A. (2009). Shock loading response of sandwich panels with 3-D woven E-glass composite skins and stitched foam core. *Composites Science and Technology*, 69(6), 736-753.  
<https://doi.org/10.1016/j.compscitech.2008.03.017>

52. Fahr, P., Yazici, M., & Shukla, A. (2018). Shock response of filled corrugated sandwich structures under extreme temperatures. *Journal of Sandwich Structures & Materials*, 20(1), 130-149. <https://doi.org/10.1177/1099636216650987>
53. Jackson, M., & Shukla, A. (2011). Performance of sandwich composites subjected to sequential impact and air blast loading. *Composites Part B: Engineering*, 42(2), 155-166. <https://doi.org/10.1016/j.compositesb.2010.09.005>
54. Hebert, M., Rousseau, C. E., & Shukla, A. (2008). Shock loading and drop weight impact response of glass reinforced polymer composites. *Composite structures*, 84(3), 199-208. <https://doi.org/10.1016/j.compstruct.2007.07.002>
55. LeBlanc, J., Gardner, N., & Shukla, A. (2013). Effect of polyurea coatings on the response of curved E-glass/vinyl ester composite panels to underwater explosive loading. *Composites Part B: Engineering*, 44(1), 565-574. <https://doi.org/10.1016/j.compositesb.2012.02.038>
56. LeBlanc, J., & Shukla, A. (2011). Response of E-glass/vinyl ester composite panels to underwater explosive loading: Effects of laminate modifications. *International Journal of Impact Engineering*, 38(10), 796-803. <https://doi.org/10.1016/j.ijimpeng.2011.05.004>
57. Dorey, G. Impact damage in composites-development, consequences, and prevention. In 'Proc. 6th Int. Conf. on Composite Materials and 2nd European Conf. on Composite Materials', Imperial College, London, 1988, Vol. 3, pp. 3.1-3.26
58. Inman, D. J., & Singh, R. C. (1994). *Engineering vibration (Vol. 3)*. Englewood Cliffs, NJ: Prentice Hall.
59. Ukyam, S.B., Mantena, R.P., Stoddard, D.L., Rajendran, A.M. and Moser, R.D. (2021) Dynamic Flexural Modulus and Low-Velocity Impact Response of Supercomposite™

Laminates with Vertical Z-Axis Milled Carbon Fiber Reinforcement. *Materials Sciences and Applications*, 12, 152-170. <https://doi.org/10.4236/msa.2021.124010>

## VITA

Shahriar Chowdhury

### EDUCATION

B.S. Mechanical Engineering  
Bangladesh University of Engineering and Technology  
Dhaka, Bangladesh

2016

### EXPERIENCE

Assistant Engineer  
Energypac Engineering Ltd.  
Dhaka, Bangladesh